

1 **Characterization of VOCs and their related atmospheric processes in a central China city**
2 **during severe ozone pollution periods**

3 Bawei Li¹, Steven Sai Hang Ho^{2,3*}, Sunling Gong^{1,4*}, Jingwei Ni¹, Huairui Li¹, Liyan Han¹, Yi
4 Yang¹, Yijin Qi¹, Dongxu Zhao¹

5 ¹ *Langfang Academy of Eco Industrialization for Wisdom Environment, Langfang 065000, China*

6 ² *Division of Atmospheric Sciences, Desert Research Institute, Reno, Nevada, USA*

7 ³ *Key Lab of Aerosol Chemistry & Physics, Institute of Earth Environment, Chinese Academy of*
8 *Sciences, Xi'an 710061, China*

9 ⁴ *Center for Atmosphere Watch and Services of CMA, Chinese Academy of Meteorological Sciences,*
10 *Beijing 100081, China*

11 *Correspondence to: Steven Sai Hang Ho (stevenho@hkpsrl.org) and Sunling Gong

12 (gongsl@cma.gov.cn)

13 Revision on: December 22, 2018

14 Abstract

15 A five-month campaign (from May to September 2017) was conducted to characterize volatile
16 organic compounds (VOCs) for the first time at four sites in Zhengzhou City, Henan Province,
17 China, where ground level ozone (O₃) concentration shown an increasing trend in recent years.
18 Canister samples were collected for measurement of fifty-seven VOCs, which, along with reactive
19 nitrogen oxides (NO_x), are the most important O₃ precursors. During the same period, O₃ and its
20 precursor gases were monitored online simultaneously. The results indicated that the average
21 mixing ratio of total quantified VOCs ($\Sigma_{\text{VOCs}} = 28.8 \pm 22.1$ ppbv) in Zhengzhou was lower than that
22 in the other Chinese megacities, while alkyne was a higher proportion of Σ_{VOCs} . The abundances,
23 compositions and ratios of typical VOCs showed clear spatial and temporal variations. Cluster
24 analysis indicates that air masses from south of Zhengzhou were cleaner than from other directions.
25 The molar ratio of VOCs to NO_x indicated that, in general, O₃ formation was more sensitive to
26 VOCs than NO_x formation in Zhengzhou. The source apportionment was conducted with Positive
27 Matrix Factorization (PMF), and it was found that vehicle exhaust, coal and biomass burning, and
28 solvent usage were the major sources for ambient VOCs at all four sites. From Potential Source
29 Contribution Function (PSCF) analysis, the strong emissions from coal+biomass burning and
30 solvent usage were concentrated in southwest of Shanxi and Henan province. The results of this
31 study gather scientific evidences on the pollution sources for Zhengzhou city, benefiting the
32 Government to establish efficient environmental control measures particularly for O₃ pollution.

33

34 1. Introduction

35 Volatile organic compounds (VOCs) are diverse and reactive chemicals. Vehicle exhausts, fuel
36 combustion and evaporation, and solvent usage are the known major anthropogenic sources of
37 VOCs (Fujita et al., 1994; US EPA, 2000; Fujita, 2001; Borbon et al., 2002). VOCs play a crucial
38 role in the ground-level ozone (O₃) pollution (Haagen-Smit, 1952; Choek and Heuss, 1987), which
39 has troubled many rapid economy-growth urban cities (Wang et al., 2017b; Nagashima et al., 2017).
40 Many related studies are thus being conducted globally (Wei et al., 2014; Malley et al., 2015; Ou et

41 al., 2015). In China, the investigations on VOCs including source apportionment, measurement of
42 emission profiles and interpretation of seasonal variations were mainly concentrated in Yangtze
43 River Delta (YRD), Pearl River Delta (PRD) and Beijing-Tianjin (BJT) regions (An et al., 2014;
44 Wang et al., 2014; Chen et al., 2014; Liu et al., 2016; Guo et al., 2017). Limited studies have been
45 conducted in less developed or developing regions (i.e., southwestern and northwestern China)
46 where prominently impacted by biomass burning and with high abundances of toxic and reactive
47 compounds (Li et al., 2014; Li et al., 2017a).

48 Fifty-seven VOCs, including C₂ - C₁₀ alkanes, alkenes, alkynes and aromatics, which greatly
49 contribute to ambient O₃ formation, have been identified and are regularly monitored by
50 Photochemical Assessment Monitoring Stations (PAMS) (US EPA, 1990; Oliver et al., 1996). Due
51 to characteristic structure and reactivity of these compounds, their contributions in O₃ production
52 varies (Carter, 1994); it has been reported that aromatics and alkenes were responsible for most of
53 the weighted reactivity of VOCs (59.4% and 25.8%, respectively) in Pearl River Delta (PRD)
54 region in China (Ou et al., 2015). Consequently, researchers have deduced that reductions of
55 alkenes and aromatics are suitable targets for O₃ control (Wang et al., 2018). In addition, with the
56 variations on energy structure, industrial construction and meteorological conditions (Shao et al.,
57 2011; Wang et al., 2015), major emission sources of VOCs at each city are unique. In less
58 developed cities of Heilongjiang and Anhui, biomass combustion had the highest contribution (40%
59 and 36%, respectively) to the O₃ formation potentials due to high quantity of agricultural activities,
60 while in the developed cities such as Shanghai, Beijing and Zhejiang, solvent usage has become a
61 more important source (Wu and Xie, 2017). Therefore, identification on district emission sources of
62 VOCs is necessary to provide scientific-based information for policy-makers who establish
63 efficient strategies to alleviate O₃ pollution.

64 In addition to the factors discussed above, non-linear relationships between ambient VOCs,
65 nitrogen oxide (NO_x) and O₃ production such that decreasing tropospheric O₃ is more complex than
66 expected (Lin et al., 1998; Hidy and Blanchard, 2015; Li et al., 2018). Many modeling and field
67 studies showed that photochemical O₃ production in several cities in China such as Guangzhou,
68 Shanghai and Beijing with high levels of NO_x were highly sensitive to VOCs (Shao et al., 2009; Ou

69 et al., 2016; Gao et al., 2017). The sensitivity regime is always varied with time and geographical
70 locations (Luecken et al., 2018). The percentage of VOC-limited regime in North China Plain (NCP)
71 increased from 4% to 6% between 2005-2013, owing to the rapid increases of NO_x emissions (Jin
72 and Holloway, 2015).

73 Zhengzhou City is an important developing city in the mid-west of the Huanghe-Huaihe river
74 flood plain in China. As the capital city of Henan Province, it is densely populated with more than
75 seven million residents in 2010 (Geng et al., 2013). With the rapid growth of industrial activities, as
76 well as increased vehicle emissions and fuel combustion, air quality in Zhengzhou has deteriorated.
77 The Air quality index (AQI) for 65% of the days in 2013 exceeded the allowable limits of 100
78 established by the Air Quality Guideline (Chinese Ministry of Environmental Protection, 2012).
79 Particularly O₃ was the major pollutant in summer and over 50% of the days in 2015, the mixing
80 ratio of O₃ exceeded the Grade I standard (100 µg m⁻³) of daily maximum average 8-hour (DMA8)
81 in Henan (Shen et al., 2017; Gong et al., 2017; Liu et al., 2018). As one of the major precursors of
82 O₃, the study on VOCs is of significance for Zhengzhou, since no related researches are published
83 in peer-reviewed literature. In this work, a comprehensive sampling campaign for VOCs
84 measurement and characterization has been conducted at four monitoring stations during the time
85 period of May - September 2017. The spatial and temporal variations in VOCs in Zhengzhou were
86 determined. The contributions of major emission sources were quantified, and the relationship
87 among O₃-VOCs-NO_x was discussed in details. The results and implications from this study can
88 provide useful guidance for policy-makers to alleviate ozone pollution in Zhengzhou, China.

89 **2. Observation and Methodology**

90 **2.1 Sampling site**

91 Based on the density of population distribution, locations of industrial facilities, and the
92 prevailing winds, four sites have been selected for sample collection: Jingkai community (JK;
93 113.73°E, 34.72°N), municipal environmental monitoring station (MEM; 113.61°E, 34.75°N),
94 Yinhang school (YH; 113.68°E, 34.80°N) and Gongshui company (GS; 113.57°E, 34.81°N), which
95 are located at the southeastern, southwestern, northeastern and northwestern of Zhengzhou,

96 respectively (Fig. 1). There is a main airport highway and heavy-traffic ring roads approximately
97 500 m west of JK. Furthermore, the site is at a distance of 2 km from an industrial area, which
98 involves packaging and printing plants, and material distribution factories. It is noteworthy that
99 there are three coal-fired power plants in the urban area of Zhengzhou city. One of the power plants
100 with the highest production was 1.6 km northwest of MEM, and MEM was surrounded by a main
101 road with four traffic lanes, the distance between the nearest traffic light and the sampling site was
102 just 200 m. Both the MEM and YH include a mix of commercial and condensed residential areas,
103 whereas the apartments around YH are more aged. The GS site is surrounded by several
104 manufacturing plants, including pharmaceuticals, materials, foods and machineries.

105 Ten dry days (i.e., no rainfall recorded) were chosen in every month during the period of May -
106 September, 2017 consequently, to represent a typical air quality condition in a month. Grab samples
107 were collected minute using 3.2 L stainless-steel canisters (Entech Instrument, Inc., Simi Valley,
108 CA, USA), which were pre-cleaned with high purity nitrogen and pressurized to 20 psi. Two
109 samples, one collected at 07:00 with increasing of human activities and another one collected at
110 14:00 with well-mixed of ambient air, were obtained on each sampling day. A total of 400 samples
111 were collected in this study. The chemical analysis was accomplished within two weeks after the
112 collection of samples. Real-time data for trace gases, including SO₂, CO, NO₂/NO_x and O₃, and
113 synchronous meteorological data, such as temperature (T), relative humidity (RH), wind direction
114 (WD) and wind speed (WS), were recorded at each air monitoring station, the message of relevant
115 equipment are listed in Table S1.

116 **2.2 Chemical Analysis**

117 In this study, the measurement of VOCs was based on Compendium Method TO-15, which
118 was established by U.S. EPA (US EPA, 1999). Air in the canister was concentrated using
119 liquid-nitrogen at -160 °C in a cryogenic pre-concentrator (7100A, Entech Instrument, Inc.). Both
120 CO₂ and H₂O were removed from the transfer line. The air was then thermally desorbed at 120 °C
121 and transferred for analysis to a gas chromatography (GC, 7890A, Agilent Technologies, Santa
122 Clara, CA, USA) coupled with dual detectors, i.e. a mass spectrometric detector (MSD) and a flame
123 ionization detector (FID) (5977E, Agilent Technology). Dual columns were applied for the

124 simultaneous analysis of C₂ - C₁₁ hydrocarbons. A PLOT column (15 m, internal diameter of 0.32
125 mm and film thickness of 3.0 μm) was connected to the FID for detection of C₂ - C₅ NMHCs,
126 whereas C₅ - C₁₀ NMHCs, oxygenated VOCs (OVOCs) and halocarbons were separated using a
127 DB-624 column (30 m×0.25 mm inner diameter × 3.0 μm film thickness), which was connected to
128 the MSD. Target compounds were identified with retention time and mass spectra, and quantified
129 with multi-point calibration curve in this study. The standard gas of PAMS (1 ppm; Spectra Gases
130 Inc, NJ, USA) was used to construct the calibration curves for the 57 target VOCs, including 28
131 alkanes, 11 alkenes, acetylene and 17 aromatics. Detailed information on the target analyses
132 involved in this study and their corresponding linearity of calibration (R²), measurement relative
133 standard deviation (RSD), method detection limit (MDL), maximum increment reactivity (MIR,
134 Carter, 2010) are presented in Table S2.

135 **2.3 Positive matrix factorization (PMF)**

136 The U.S. EPA PMF 5.0 software was used for source apportionment (Lau et al., 2010; Abeleira
137 et al., 2017; Xue et al., 2017). Due to the complex chemical reactions, the application of PMF in
138 VOCs has to be based on a couple of principles: eliminating species with mixing ratios below MDL
139 and excluding species with high reactivity, except for the source markers (Guo et al., 2011; Shao et
140 al., 2016). Finally, 31 VOC species and NO₂ were chosen for the source apportionment analysis.

141 In this study, PMF was performed with fifty base runs for each site, results with the minimum
142 Q value (a parameter used to express uncertainties of PMF results) were considered as optimum
143 solutions. In Table S3 the r² between observed values and predicted values of selected VOCs and
144 NO₂ are presented for the four sites, the r² for most species (> 80%) were higher than 0.6,
145 compounds with r² < 0.6 were down weighted when determine factor sources.

146 During PMF analysis, bootstrap method was used to evaluate stability and uncertainty of the
147 base run solution, setting the minimum correlation coefficient r² at 0.6, 100 bootstrap runs were
148 performed, and the results were showing in Table S4, and acceptable results (> 80%) were gained
149 for all the factors.

150 Three to nine factors were selected to initiate the running of PMF, the Q/Q(exp) for every site
 151 at fixed factor size were presented in Table S5. With the increase of factor number, the ratios
 152 Q/Q(exp) were declined due to additional factors. When the factor size changing from 3 to 4, 4 to 5,
 153 and 5 to 6, the decrement of Q/Q(exp) were larger (~18-25%), while the change was lower than 12%
 154 after factors increased to 7, combined with the field conditions, six factors were defined at each
 155 site.

156 2.4 Potential source contribution function (PSCF)

157 In this trajectory-based study, the probability of air clusters with source concentration higher
 158 than a certain value was estimated (Hopke et al., 1995). Briefly, the PSCF value in ij^{th} grid was the
 159 ratio of the number of endpoints with higher source concentration relative to the total number of
 160 endpoints in ij^{th} grid cell. The criterion value, equal to 75th percentile of the targeted source
 161 concentration in this study, was used to verdict whether the value was higher or not. The 48-hour
 162 back trajectories was calculated with Hybrid Single-Particle Lagrangian Integrated Trajectory
 163 (HYSPLIT) model. Because there are many grid cells with small values, which could result in high
 164 uncertainty, a weighting function (W_{ij}) was introduced results (WPSCF) (Polissar et al., 1999).
 165 According to average values of end points in each cell, in this case, W_{ij} was presented as below.

$$W_{ij} = \begin{cases} 1.0 & n_{ij} > 30 \\ 0.7 & 10 < n_{ij} \leq 30 \\ 0.42 & 5 < n_{ij} \leq 10 \\ 0.05 & n_{ij} \leq 5 \end{cases}$$

166 167 2.5 Estimation of the initial NO_x and VOCs

168 With the assumption that chemical loss of NO_x and VOCs were mainly due to their reactions
 169 with hydroxyl radical ($\bullet\text{OH}$), the initial mixing ratio of NO_x can be calculated with the equation as
 170 (Shiu et al., 2007; Shao et al., 2009):

$$171 \quad [\text{NO}_x] = [\text{NO}_x]_0 \exp(-k [\bullet\text{OH}] \Delta t) \quad (1)$$

172 where k stands for the reaction rate between NO_x and $\bullet\text{OH}$. In this study, k was set as the product of
173 the rate constant for $\text{NO}_2+\bullet\text{OH}$ multiplied by the observed average ratio of NO_2/NO_x during this
174 campaign.

175 The photochemical age (Δt) can be estimated from the ratio between two compounds, emitted
176 from a common source, but having different reaction rate with $\bullet\text{OH}$. For this case, the
177 photochemical age clock was performed with ethylbenzene (E) and m,p-xylene (X) (Sun et al.,
178 2016).

$$179 \quad [\bullet\text{OH}] \Delta t = 1/(k_x - k_E) [\ln(X_0/E_0) - \ln(C_X/C_E)] \quad (2)$$

180 which k_x and k_E represent their rate constants with $\bullet\text{OH}$, C_X and C_E correspond to the observed
181 mixing ratios; X_0 and E_0 were their initial concentrations. The X_0/E_0 was estimated from the 5th
182 percentile of the observed ratios at 07:00 in this paper.

183 The initial mixing ratio of VOC was estimated with the same method as for NO_x (Shiu et al.,
184 2007):

$$185 \quad [\text{VOC}]_0 = [\text{VOC}]_t \exp(k_i [\bullet\text{OH}] \Delta t) \quad (3)$$

186 where $[\text{VOC}]_t$ was the observed mixing ratio of i^{th} species and k_i was the correspondent rate
187 constant with $\bullet\text{OH}$.

188 **3 Results and discussions**

189 **3.1 Meteorological variations and Mixing ratios**

190 Meteorological conditions are important factors that impact both the compositions and levels of
191 VOCs. During the sampling period, the T varied from 15 to 38°C, RH varied from 38 to 100% (Fig.
192 S1), and the dominant winds were northwestern and southeastern (Fig. 2). The air clusters, analyzed
193 by HYSPLIT model, showed moderate differences in each month (Fig. 3). In May, clusters arriving
194 at Zhengzhou demonstrated longer paths, and included six clusters in total, while in June, the length
195 of clusters were shorter. However, the concentration levels and compositions of VOCs were similar
196 in the two months. In May, the largest cluster (27.2%) was passed over from Yinchuan, a central
197 city in northwest China, then crossing several non-capital cities (i.e., Yanan, Yuncheng and

198 Luoyang) in Shanxi and Sichuan provinces. Such a long-range transport of pollutants has less
199 impact on the air quality of Zhengzhou, as comparable level and similar compositions of VOCs
200 were obtained during the period of May - June. In June, August and September, approximately half
201 of the air trajectories originated from the areas of Henan province, indicating the air pollutants in
202 Zhengzhou were impacted by local factors.

203 The total concentrations of VOCs (Σ_{VOCs}) are presented in Table 1. The Σ_{VOCs} varied at the four
204 sites, where the highest Σ_{VOCs} and their compositions were not identical across the sampling months
205 as well. In May 2017, the highest Σ_{VOCs} was reported at JK (37.6 ± 22.6 ppbv), followed by GS
206 (31.7 ± 18.7 ppbv), YH (30.1 ± 16.4 ppbv) and MEM (29.1 ± 15.3 ppbv), while the Σ_{VOCs} values for
207 the month of June, July, August and September were found to be in the order of: GS > JK > MEM >
208 YH, MEM > GS > JK > YH, YH > MEM > JK > GS, and MEM > YH > GS > JK, respectively.
209 This can be attributed to numerous factors that will be explored later in the paper.

210 Besides the emission sources (to be discussed in Section 3.2), the impacts controlled by
211 meteorological conditions should not be ignored as well. For instance, the prevailing wind in May
212 was northwestern at GS and YH, while the southwestern wind was dominant at JK (Fig. 4). The
213 transport of air pollutants from urban center and industrial plants should be resulted in the highest
214 level of Σ_{VOCs} at JK. In June 2017, the prevailing wind was southeastern at MEM, YH and GS (Fig.
215 4). The average wind speed at GS (0.74 ± 0.33 m s⁻¹) was lower than that at MEM (1.84 ± 0.94 m s⁻¹)
216 and YH (0.97 ± 0.36 m s⁻¹) (Table 2), indicating poor dispersion conditions at GS. The air pollutants
217 emitted from MEM and YH were more liable resulting in a higher level of Σ_{VOCs} at GS in June. It
218 should be noted that, when Σ_{VOCs} at JK was higher than that of GS, the level at YH was higher than
219 that of MEM, and vice versa. Except for the discriminations between the pollution sources at every
220 site, there may be some other factors (e.g. horizontal and vertical air advection) contribute to it.

221 Due to the variations of the planet boundary layer (PBL) height, solar radiation and emission
222 sources, the concentrations of VOCs displayed obvious differences between morning and afternoon
223 time (07:00 LT and 14:00 LT in this study). Compared with morning period, the aromatic
224 compounds showed lower compositions at 14:00 LT (Fig. 5), because of the increased planet
225 boundary layer and the active photochemical reactions, while alkenes always peaked in the 14:00

226 LT. According to the dataset, the increases in alkene compositions (~4.3% uplift) were mainly due
227 to higher contributions of isoprene (~1.4% at morning and 7.6% in the afternoon), which was
228 mainly emitted from biogenic sources and increased exponentially with ambient temperature
229 (Guenther et al., 1993; Guenther et al., 1995).

230 The average Σ_{VOCs} values in Zhengzhou (28.8 ± 22.1 ppbv) were significantly lower than those
231 in Beijing (65.6 ppbv), Hangzhou (55.9 ppbv), Guangzhou (47.3 ppbv) and Nanjing (43.5 ppbv),
232 and higher than that in Wuhan (23.3 ± 0.5 ppbv) (Table 3). Factors, including population density,
233 industrial activity, fuel composition, local stringent regulations for environmental protection, terrain,
234 and weather are the potential reasons for the differences in VOCs concentrations in those cities.
235 With regard to the weight percentage of major groups (Table 3), the composition of alkanes was the
236 largest in all cities because of their longer lifetimes and widespread sources (Fig. 5), while the
237 composition of aromatics was lower than alkenes in these cities except for Guangzhou. It is well
238 known that aromatics mainly originate from solvent usage and vehicle exhaust in summer. The
239 large amount of shoemaking and shipbuilding industries involving large amounts of solvent usage
240 may be the main reason for the higher composition of aromatics in Guangzhou. In comparison with
241 other four cities, the composition of aromatics in Zhengzhou was the lowest probably due to its less
242 solvent-used manufacturers than in Guangzhou, Hangzhou and Nanjing, and less numbers of
243 vehicles than in Beijing. Alkyne contributes least to VOCs in cities listed in Table 3, with higher
244 level observed in Zhengzhou, where ranked second after Hangzhou. Alkyne typically originates
245 from combustion sources. Zhu et al. (2016) observed that the composition of alkyne in the
246 biomass-burning period could be double of that in the non-biomass burning period (Zhu et al.,
247 2016). As Henan is the largest agricultural province in China and the sampling duration covered the
248 crop harvest season, the residents often used crop residues as the biofuel for their subsistence and a
249 higher alkyne composition in Zhengzhou was thus resulted.

250 **3.2 Temporal variations**

251 The time series of mixing ratios of NO_x , O_3 and Σ_{VOCs} at every site are shown in Fig. 6. The
252 results showed a distinctive temporal characteristic where lower levels of SO_2 , CO, NO_x , O_3 and
253 Σ_{VOCs} were observed in July and August (mid-summer) (Table S6). These results were similar to

254 those obtained for other urban areas worldwide (Cheng et al., 1997; Na et al., 2001; Li and Wang,
255 2012). Changes in PBL height, human activities, and abundance of $\bullet\text{OH}$ were the potential causes
256 for the phenomenon. The occurrence of precipitation, which is usually accompanied with better air
257 dispersion conditions, is also frequent in most areas of China during summer, resulting in
258 decreasing background level of air pollutants. Additionally, a series of effective local policies, such
259 as prohibition of painting and coating in open air and limitations on fuel supply between 10:00
260 -17:00 LT during hot summer days assisted in suppressing the emissions of VOCs. Meanwhile,
261 many organizations, such as schools, institutes and scattered private workshops, were closed due to
262 summer vacations. Some large-scale industries also stopped manufacturing processes for two weeks
263 during this period. Consequently, the anthropogenic emissions were reduced, which in turn resulted
264 in a decrease in VOCs, SO_2 , and NO_x emissions. The reduction of precursor levels and unfavorable
265 photochemical conditions (such as, higher RH) resulted in the lower O_3 levels in July and August.

266 Beside local emissions, the long-range air mass also had some impacts on relatively lower
267 level of Σ_{VOCs} in July. As illustrated in Fig. 3, different from other months, the air current was
268 originated with the largest portion (*ca.* 88.7%) of clusters from Hubei province, where the average
269 Σ_{VOCs} in its capital city (23.3 ± 0.6 ppbv) (Lyu et al., 2016) was lower than that in Zhengzhou
270 (29.2 ± 23.1 ppbv). In combination with the lower weight percentage of photochemically-reactive
271 aromatics ($10.3 \pm 4.2\%$), and the lowest toluene to benzene (T/B) ratio of 1.15 ± 0.99 around this
272 period, it is possible that the cleaner air mass clusters originating from Hubei also contributed to the
273 reduction of Σ_{VOCs} in July.

274 As demonstrated in Fig. 6, the observed Σ_{VOCs} values at 07:00 LT were often higher than those
275 at 14:00 LT. The accumulation of pollutants during night-time and the temperature inversion in the
276 morning were the most reasonable explanations for this phenomenon. Stronger photochemical
277 reaction during noon-time led to the reduction in atmospheric VOCs. It should be noted that
278 pronounced Σ_{VOCs} were occasionally observed at MEM and GS (Fig. 7), which were potentially
279 ascribed to sharp changes in local emissions and meteorological conditions. Specifically, at MEM,
280 the distinctive increment was always accompanied with obvious increases of alkanes or aromatics
281 (Fig. 7). Since the T and RH were often consistent during the sampling period, the direct gas

282 evaporations should be constant as well. Therefore, the simultaneous increased concentrations of
283 SO₂, CO and NO_x could illustrate the potential impacts from combustion sources, such as emissions
284 from nearby thermal power plant. At GS, the increase of ΣVOCs in June was usually with extremely
285 high levels of aromatics, due to the disturbance from solvent use for building renovation during this
286 period, and the abnormal high levels of ΣVOCs in other months were related to the rising
287 concentrations of C₃-C₄ alkanes, which were mainly originated from consumptions of compressed
288 natural gas (CNG) or LPG (Huang et al., 2015). The results support the possible impact from a
289 gas-fueled power plant located about 1 km southwest of the site (~18% of prevailing western wind
290 at GS during May to September).

291 It is of interest to note that on the morning of 5th September, acetylene was found in extremely
292 high concentrations (14.7 - 39.4 ppbv). Its mixing ratio in most of the urban areas was < 10 ppbv
293 (Duan et al., 2008; Guo et al., 2012; Louie et al., 2013). 5th September is a festival day for the
294 people who worship their ancestors. A large number of incenses and offerings, made up of wood
295 and paper, were burnt during the festival, resulting in an elevation of acetylene all over the
296 Zhengzhou city (Zhu et al., 2016).

297 **3.3 Spatial variations**

298 The C₂ - C₅ alkanes, acetylene, ethylene, toluene and benzene were the most abundant VOCs
299 detected at all sites (Fig. 8), and the mixing ratios of toluene varied within a wide range at each site,
300 because of its universal emission sources (e.g., vehicle exhaust emissions and solvent usage)
301 (Barletta et al., 2005; Wang et al., 2014). These chemicals contributed > 60% for ΣVOCs at each site,
302 illustrating strong combustion-related sources in Zhengzhou.

303 Among the four major organic classes, alkane was the most abundant group as a result of its
304 widespread sources and longevity (Fig. 5), accounted for 52.9%, 62.5%, 53.4%, 53.4% of the total
305 ΣVOCs at JK, MEM, GS, and YH, respectively. The highest composition of alkane was observed at
306 MEM due to the stronger contributions of ethane, iso-pentane, and C₆-C₈ branched alkanes (Fig.
307 S3), which are emitted from light-duty gasoline vehicles (Wang et al., 2017a).

308 The average Σ_{VOCs} were slightly higher at industrially impacted sites of GS (31.7 ± 28.7 ppbv)
309 and JK (28.6 ± 22.0 ppbv) than those at MEM and YH (Fig. 9). Additionally, the air pollutants
310 related to the combustion processes, such as SO_2 and CO, were marginally more abundant, in
311 western areas of Zhengzhou (GS and MEM) (Fig. 9). Under high levels of VOCs and sufficient
312 supply of NO_x , the highest average mixing ratio of O_3 was observed at GS, followed by YH where
313 even with, which had the lowest VOCs and NO_x , indicating that there are multiple factors, rather
314 than the absolute concentrations, contributing to the formation of the secondary pollutant, O_3 at
315 YH.

316 In June, the O_3 concentration often exceeded the national standard level of 80 ppbv, i.e., there
317 was severe air pollution during this period. The average mixing ratio of O_3 during daytime
318 (07:00-18:00 LT) in June, 2017 at JK, MEM, YH, and GS were 74.9 ± 39.6 ppbv, 73.5 ± 40.6 ppbv,
319 73.8 ± 35.7 ppbv, and 88.0 ± 46.1 ppbv, respectively (Table 4). The higher level of O_3 at GS was
320 accompanied with the higher Σ_{VOCs} (39.3 ± 25.4 ppbv). The weight percentage of aromatics ($15.6 \pm$
321 12.1%) at GS was higher than those at other sites as well, indicating that the painting and other
322 renovation activities at GS was potentially an important factor for its high O_3 level in June. Even
323 though both the Σ_{VOCs} and specifically high O_3 formation potential compounds (such as alkenes and
324 aromatics) at MEM were slightly higher than those at YH (Table 4), the O_3 concentration at MEM
325 was not higher. This could be attributed to other critical precursors such as NO. NO at MEM (7.72
326 ppbv) was significantly higher than that at YH (2.57 ppbv) during daytime, indicating that the
327 titration reaction between O_3 and NO was more efficient at MEM.

328 Because photochemistry producing O_3 occurs over several hours to days, O_3 episodes are
329 attributable not only to local sources but also to regional transports. For example, Streets et al.
330 (2007) reported that with continuous southern winds, the O_3 level in Beijing was 20-30%
331 contributed from its neighboring cities in Hebei. During our study, a typical regional ozone
332 pollution was happened on August 10th at YH (Fig. 6). On that day, the ratios of VOCs/ NO_x at the
333 four sites were all less than 6.5 (ppbC/ppbv) (Fig. S4), indicating a regional VOC-control system,
334 and that VOCs are the critical contributors to the formation of O_3 in Zhengzhou. The reductions in
335 Σ_{VOCs} in the afternoons (around 14:00 LT) compared to mornings (around 07:00 LT) may have

336 been due, in part, to chemical loss of VOC as O₃ is formed. The reduction of ΣVOCs and active
337 compounds (i.e., aromatic+alkene) at 14:00 relative to 07:00, 35% and 56% respectively, was least
338 at YH among the four sites (Fig. S4). Based on the wind direction, between 08:00 - 15:00 LT on
339 August 10th, YH was downwind of the other three sites (Fig. S4). All of this confirms that the
340 abnormally high O₃ at YH was caused by the transport of air pollutants from other sites on that day.

341 **3.4 VOCs/NO_x ratio**

342 The VOCs/NO_x ratio is often used to distinguish whether a region is VOCs or NO_x limited in
343 O₃ formation. Generally, VOC-sensitive regimes occur when, with VOCs/NO_x ratios are lower than
344 10 in the morning; NO_x-sensitive regimes occur when VOCs/NO_x ratios are greater than 20 (Hanna
345 et al., 1996; Sillman, 1999). In this study, the mean value of VOCs/NO_x (ppbC/ppbv) were below 5
346 at all four sites (Fig. 10), and 75% of the data points were < 6, indicating that the O₃ formation was
347 sensitive to VOCs in Zhengzhou, and the reductions on the emissions of VOCs will be a benefit for
348 O₃ alleviation.

349 The VOCs/NO_x showed differences among the four sites (Fig. 10), with the lowest value at
350 MEM (~3.8) and the highest value at JK (~4.7). The production of O₃ at MEM is more sensitive to
351 VOCs than at JK due to presence of strong NO_x emissions from a thermal-power plant.
352 Approximately 14% of the measured VOCs/NO_x ratios of > 8.0 were found in the NO_x-limited site
353 of JK, resulting from higher VOCs or lower NO_x emissions than at other sites. Both of the mixing
354 ratios and the statistical data showed higher levels of VOCs (with lower NO_x) at GS, where only ~4%
355 of the ratios of > 8.0 was observed, indicating that there must be other factors (unresolved in this
356 study) impacted the variation of O₃ formation regimes.

357 From the daily variations of VOCs/NO_x ratios (Fig. 10), higher values were observed at 14:00
358 LT than at 07:00 LT at all four sites, well correlated with less vehicle emissions or more
359 consumption paths for NO_x with stronger light intensity. The increment of VOCs/NO_x at 14:00 LT
360 was more obvious at JK and GS, suggesting that more emission sources of VOCs at daytime, and
361 resulting the O₃ formation system shifting to the transition area in the afternoon.

362 O₃ formation depends not only on the abundances of precursors (mainly VOCs and NO_x) but
363 also VOCs to NO_x ratio (Sillman, 1999; Pollack et al., 2013). In this research, the mixing ratio of
364 O₃ at 14:00 LT presented a slightly positive trend ($p < 0.05$) with the uplift of VOCs/NO_x at JK (Fig.
365 11), consistent to the results observed at the megacity of Shanghai (Gao et al., 2017), where the O₃
366 formation was more sensitive to NO_x when high O₃ levels were observed. Without considering the
367 advection of air parcels, this can be attributed to the increased O₃ production efficiency at high
368 VOCs/NO_x. There were no discernible trends at other sites, possibly due to the counteraction
369 imposed by other uncertain factors.

370 3.5 Ratios of specific compounds

371 Ratios of specific VOCs are useful to identify emission sources (Ho et al., 2009; Liu et al.,
372 2015; Raysoni et al., 2017). In order to characterize the differences in the contribution of various
373 sources at each site, ratios of i-pentane/n-pentane and toluene/benzene (T/B) ratios are discussed
374 here.

375 The ratio of i-pentane to n-pentane can be used to differentiate potential sources such as
376 consumption of natural gas, vehicle emissions and fuel evaporations. In areas heavily impacted by
377 natural gas drilling, the ratios lie in the range of 0.82 - 0.89 (Gilman et al., 2013; Abeleira et al.,
378 2017). Higher values are often reported for automobiles: in a range of 2.2 - 3.8 for vehicle
379 emissions; and 1.8 - 4.6 for fuel evaporation (McGaughey et al., 2004; Jobson et al., 2004; Russo et
380 al., 2010; Wang et al., 2013), whereas the ratios below unity was found for coal combustion (0.56 -
381 0.80) (Yan et al., 2017).

382 In this study, i-pentane and n-pentane were highly correlated ($R^2=0.87 - 0.94$) throughout the
383 whole sampling campaign (Fig. 12), indicating constant pollution sources for these two compounds.
384 The highest ratio of i/n-pentane was found at JK (2.59 ± 0.45), which was comparable to the value
385 of 2.93 reported in a Pearl River Tunnel (Liu et al., 2008), thus indicating strong impacts from
386 traffic-related sources. The average ratio at MEM was 2.31 ± 0.68 , higher than the character ratios
387 of coal combustion, reasonably due to the observation site presented at upwind position of the
388 thermal power plant. And frequent idling may cover up the contribution from coal combustion,

389 reflecting the impact of traffic emissions. The average ratios at YH (1.94 ± 0.57) and GS ($1.63 \pm$
390 0.51) were lower than those at the above two sites, suggesting the comparatively stronger
391 contribution from coal burning.

392 Tunnel and roadside researches indicates that T/B ratio varies within the range of 1 - 2 when
393 the atmosphere is heavily impacted by vehicle emissions (Wang et al., 2002; Tang et al., 2007;
394 Gentner et al., 2013; Huang et al., 2015). The ratio of < 0.6 was ascribed to other sources such as
395 coal combustion and biomass burning (Tsai et al., 2003; Akagi et al., 2011). The industrial activity
396 would be more dominant when the T/B ratio is greater than 3 (Zhang et al., 2015).

397 In this study, the correlation between benzene and toluene was fairly well at all the sites
398 ($R^2=0.70-0.74$), except for YH ($R^2=0.41$) (Fig. 14), suggesting the similar sources for benzene and
399 toluene at JK, MEM and GS, while more complex such as variable wind direction at YH. The
400 average ratios of T/B were lied within the range of 1.64-2.29, which were scattered around the
401 character ratio of 2 for vehicle exhaust, illustrating the significance of vehicle emissions at the four
402 sites. Specifically, at JK, MEM and YH, most of T/B ratios were distributed between 0.6 and 3,
403 which were corresponding to character ratios for coal or biomass burning and industrial activities
404 respectively. These reflected the mixture impacts from mobile source and coal/biomass burning at
405 these three sites. However, more values were greater than 3 at GS, suggesting more frequent
406 disturbance from industrial activities at this site.

407 The T/B ratios at 14:00 LT were lower than at 07:00 LT (Fig. 15). The reaction rate constant
408 of toluene ($5.63 \times 10^{-12} \text{cm}^3 \text{molecule}^{-1} \text{s}^{-1}$) with $\bullet\text{OH}$ is higher than that for benzene ($1.22 \times$
409 $10^{-12} \text{cm}^3 \text{molecule}^{-1} \text{s}^{-1}$), indicating more rapid consumption of toluene from photochemical reactions
410 and thus resulting in lower T/B ratios at 14:00 LT, all else being equal. The emission strength of
411 mobile source is often weaker at 14:00 LT, while the coal/biomass burning are increased due to
412 more human activities. Both chemistry and emissions offer an explanation of the lower T/B ratios
413 observed at 14:00 LT. In comparison with other months, higher T/B ratios were found more
414 frequently in September, potentially showing increased industrial activities during this period.

415 Overall, based on the iso-pentane/i-pentane and T/B ratios, the atmospheric VOCs at every site
416 were impacted by a mix of coal/biomass burning and vehicle emissions, whereas GS was more
417 liable impacted by industry-related sources.

418 3.6 Relative reactivity of VOCs

419 The reactivity of individual species is different, and in mixtures of VOCs there is competition
420 for reaction partners, leading to variations in reaction pathways and O₃ formation yields. Ozone
421 formation potential (OFP) is a useful tool to estimate maximum O₃ productions of each compound
422 under optimum conditions, from which the most important species for O₃ formation could be
423 identified (Carter, 1994). The calculation of OFP is based on mixing ratios and maximum
424 incremental reactivity (MIR) of each individual compound, Eq. (4).

$$425 \text{OFP} = C_i \times \text{MIR} \quad (4)$$

426 where C_i represents the concentration level of i^{th} species, while MIR is a constant taken from (Carter,
427 2010) (Table S2).

428 In Zhengzhou city, alkenes contribute most ($55.9 \pm 14.2\%$) to the sum of OFP, of which
429 ethylene had the largest portion. The results is different with the estimation based on emission
430 inventories by Wu and Xie (2017), in which the largest contributor of total OFP in North China
431 Plain (NCP), YRD and PRD was aromatics, reflecting that there was relatively less surface coating
432 industries in Zhengzhou.

433 For the individual species, the top 10 most contributors in OFP included ethylene, isoprene,
434 m,p-xylene, toluene, propylene, acetylene, n-butane, i-pentane and propane. Their contributions to
435 the sum of OFP was lied within the range of 69.4 - 77.6% (Table 5), with 61.3-76.5% of total
436 VOCs weighted in concentration, highlighting the importance of reduction on emissions of these
437 VOCs no matter based on relative reactivity or mixing ratios. Additionally, it is worth noting that,
438 the percentage of acetylene ($4.51 \pm 0.34\%$) weighted in OFP was higher than many other areas in
439 China, including Guangzhou (2.20%) and YRD (2.37%) (Li and Wang, 2012; Jia et al., 2016),
440 demonstrating that it is necessary to conduct emission controls on sources related to combustion
441 (i.e., vehicle emissions and biofuel burning) in Zhengzhou city.

442 Zhengzhou was suffered from the severest O₃ pollution in June, 2017. The relationships
443 between OFP of each organic group, Σ_{VOCs} , and the ambient concentrations of NO_x and O₃, as well
444 as the corresponding meteorological conditions, are shown in Fig. S5-6. At 07:00 LT, generally
445 lower WS was seen than that at 14:00 LT, offered a favorite condition for local O₃ propagation.
446 Under low RHs and high T and OFP (88.1±30.3 ppbv), the O₃ level at YH was unexpectedly lower
447 than that at MEM on sunny days. Since the OFP was estimated with the assumption of reactions
448 that proceeded under optimum conditions, the above phenomenon reflected there were unsatisfied
449 O₃ formation conditions at YH. The highest total OFP was seen at JK in June, while the highest O₃
450 levels was observed at GS where located at a downwind position with lowest WS (0.74±0.33 m s⁻¹).
451 The concentration level of O₃ usually increased with wind speed (Fig. S7), particularly when the
452 eastern wind was dominant, illustrating the disturbance from long-distance sources to urban center.

453 3.7 Source apportionment

454 The factor profiles given by PMF for each site were presented in Fig. 15. The six factors were
455 resolved as vehicle emissions, coal+biomass burning, solvent use, oil evaporation, petrochemical
456 and biogenic source (detailed characterization can be referred to supporting information) on the
457 base of the correspondent markers for each source categories, which were summarized in Table S7.
458 Meanwhile, the correlation coefficients, expressed in Pearson's *r*, were varied from 0.54 to 0.62
459 and 0.66 to 0.73 for SO₂ with coal+biomass burning, and NO₂ with vehicle emission, respectively
460 (Fig. 16), proved the precise results gained in this study.

461 The weight percentage of each factor calculated with two criteria (absolute concentrations and
462 OFPs) at the four sites were presented in Fig. 17. At every site, vehicle emission, coal+biomass
463 burning and solvent use were the top three contributors to VOCs abundance in ambient air.
464 Compared to JK and YH, even though the distances between thermal power plant and the
465 observation site was the shortest at MEM, vehicle emission (36.8%) showed the largest portion
466 instead. Coal+biomass burning (30.6%) had the highest contribution at GS, attributed to its
467 downwind position and nearby suburbs that biomass burning occurred more frequently. The
468 contributions from vehicle emission at the two urban centers of MEM (36.8%) and YH (37.4%)
469 were comparable, but higher than those at JK and YH. The consumptions of solvent at GS (18.9%)

470 and JK (14.9%) were higher than those at YH (10.1%) and MEM (11.5%), due to restriction on
471 development of new industrial enterprises in urban center in recent years. Emissions from oil
472 evaporation, petrochemical and biogenic emission were scarce, and their contributions were below
473 10% at every site.

474 On the base of O₃ formation impact, coal+biomass burning, solvent use, and vehicle emission
475 were the three major contributors as well. In contrast to the concentration weighted method, the
476 importance of solvent use estimated with OFP increased 28-65% for each site, and the significance
477 of vehicle emissions decreased 29-53%. At YH and GS, small discrimination (< 4%) in
478 contributions of coal+biomass burning between the two methods were found. On the other hand,
479 the variations on coal+biomass burning at JK (a decline of 17%) and MEM (an increase of 29%)
480 were more obvious, due to low abundance of reactive species in this factor at JK and high level of
481 alkenes at MEM. Considering that the aging index of xylene/ethylbenzene was high at MEM (2.97)
482 and low at JK (0.01) remarkably, demonstrating that the emission sources related to coal+biomass
483 burning was fresher at MEM than JK.

484 Except for oil gas evaporation and biogenic sources, in which major emitted compounds with
485 shorter life span, potential source regions for the other four identified sources (i.e., coal+biomass
486 burning, vehicle emission, solvent usage and petrochemical) apportioned by PSCF method were
487 presented in Fig. 18. Southwest of Shanxi province, western of Shandong province, and southwest
488 of Henan province were identified as hot spots for the coal+biomass burning. The active emission
489 areas for solvent use were concentrated in Henan province, and mainly located in southwest of
490 Zhengzhou. The most contribution area for petrochemical was found in southwest of both Shanxi
491 and Henan, northwest of Anhui, and southeast of Hubei provinces. For vehicle emissions, the
492 strongest emission point was scattered in southwest of Henan, while Shandong, Anhui and Hubei
493 provinces also distributed with strong emission points.

494 **3.8 Consumption of VOCs and correlations with ozone level**

495 The consumption of a VOC in the atmosphere could be presented as the difference from its
496 initial mixing ratio and the observed value following an air parcel. In isolated stagnant air, the rate

497 of change of VOC concentrations will be the sum of emissions, deposition, and chemical
498 production and loss processes.

499 The average value of VOC consumption at urban center (MEM and YH, 4-6 ppbv) was lower
500 than that in outer areas (JK and GS, 9-11 ppbv), and the average increment of O₃ at 14:00 LT was
501 higher than that at 07:00 LT in marginal area, suggesting more efficient photochemical reactions at
502 JK and GS. Meanwhile, the average values of [\bullet OH] Δt for each site, ranked in the same order with
503 VOCs consumption, were varied in a range of 2.9×10^{10} to $4.7 \times 10^{10} \text{ cm}^{-3} \text{ s}$. The values were
504 slightly lower than the results of $4.9 \times 10^{10} \text{ cm}^{-3} \text{ s}$ measured at Beijing in August-September, 2010
505 (Yuan et al., 2012), indicating that comparatively less aging process in Zhengzhou.

506 Taken the decrement of VOCs and NO_x as independent variable and the increment of O₃ as
507 dependent variable, the multiple regression analysis was performed. The results for JK and GS were
508 presented as:

$$509 \quad [\text{O}_3]_{\text{increment}} = 0.41[\text{VOC}]_{\text{decrement}} + 0.20[\text{NO}_x]_{\text{decrement}} + 53.4 \quad (\text{JK}, R^2 = 0.44)$$

$$510 \quad [\text{O}_3]_{\text{increment}} = 0.34[\text{VOC}]_{\text{decrement}} + 0.39[\text{NO}_x]_{\text{decrement}} + 59.3 \quad (\text{GS}, R^2 = 0.38)$$

511 The F values for JK and GS were 16.1 and 10.1 respectively, indicating the regression results
512 at the two sites were acceptable. However, the relationships among O₃, NO_x and VOCs could not
513 be expressed in this way at MEM and YH, where the low values for both R² (0.12, 0.09) and F
514 values (2.7, 2.8). This potentially attributed to more constant disturbance from fresh emission
515 sources at urban center.

516 **4. Conclusions**

517 In this study, VOC samples were collected at four sites in Zhengzhou, Henan (China) for the
518 first time and analyzed for 57 species. It is found that the weighted percentage of aromatics was
519 lower, while alkyne was higher in Zhengzhou city than in other Chinese cities. C₂ - C₅ alkanes,
520 acetylene, ethylene, toluene and benzene were the most abundant VOCs in the region, suggesting
521 widespread combustion-related sources in the city. Median concentrations for the four sites are
522 almost indistinguishable but, based on monthly averages, the maximum Σ_{VOCs} was observed at GS

523 site, because it is occasionally impacted by emissions from the nearby gas fueled plant, which
524 strongly skew the distribution of measured VOC concentrations. Approximately 75% of VOCs/NO_x
525 ratios were below 6 at each site, indicating that the O₃ formation was driven by VOCs regionally.
526 Different from other megacities, alkenes were the biggest contributors to OFP, and acetylene was
527 particularly critical at each site. In addition, the impact of aging process was less in Zhengzhou than
528 that Beijing. Photochemical processing appears to be more efficient at JK and GS, while the
529 relationships among O₃, NO_x and VOCs at urban sites of MEM and YH were more complex.

530 Our analysis of ozone formation does not take into account the important effects of transport
531 and mixing, and should be viewed in this light. Both measured mixing ratios and calculated OFPs
532 demonstrated that the most important contributors to VOCs were vehicle exhaust, coal+biomass
533 burning and solvent use, illustrating the necessary to conduct emission controls on these pollution
534 sources. Vehicle emission was more dominant at urban center (YH and MEM), while solvent use
535 was more important at the sites (JK and GS) far away from urban center in Zhengzhou. It is further
536 shown that the air pollution in Zhengzhou was usually impacted by local emissions, with no more
537 than 50% of 48-hour backward trajectories extended out of Henan province in June, August and
538 September, and southern air clusters occasionally from Hubei Province was cleaner. In addition,
539 strong emissions for coal+biomass burning were concentrated in southwest of Shanxi, western of
540 Shandong and southwest of Henan provinces according to the PSCF analysis. Due to less
541 anthropogenic emissions and more favorable dispersion conditions, most of the air pollutants had
542 the lowest levels in the mid-summer month of July. This study provides the first-hand information
543 on the characteristics of VOCs and assists in overcoming the O₃ pollution issue in Zhengzhou city,
544 China.

545 **Acknowledgements**

546 The authors would like to thank for valuable suggestions, corrections, and discussions from
547 both anonymous referees and editor, Prof. Rob MacKenzie. Their comments are particularly
548 important and greatly contributed to improve this work. This research was supported by the Key
549 Program of National Natural Science Foundation of China (Grant No. 91744209).

550 **Table & Figure**

551 Table 1. Mean concentrations of Σ_{VOCs} (ppbv) and correspondent standard deviations (SD) at every site during the
 552 sampling period

	JK		MEM		GS		YH	
	Mean	SD	Mean	SD	Mean	SD	Mean	SD
May.2017	37.6	22.6	29.3	15.3	31.7	18.7	30.1	16.4
June.2017	34.0	19.9	30.3	12.8	39.3	25.4	28.3	11.9
July.2017	16.0	6.1	20.7	12.7	19.6	13.9	15.9	7.5
Aug.2017	21.5	15.3	24.4	20.8	20.5	15.7	26.1	17.0
Sept.2017	26.2	16.2	34.2	23.8	30.4	19.8	32.6	19.8

553

554 Table 2. Wind speed (m s^{-1}) measured about 10m above ground level at every site during the sampling period

	JK	MEM	YH	GS
May	1.34±0.65	1.86±1.19	1.27±0.66	0.97±0.49
June	1.07±0.48	1.86±0.94	0.97±0.36	0.74±0.33
July	1.48±0.59	2.62±1.19	1.15±0.45	0.90±0.32
August	1.06±0.48	1.86±0.94	0.95±0.39	0.76±0.35
September	0.80±0.38	1.24±0.80	0.82±0.43	0.62±0.38

555

556

Table 3. Concentration levels of VOCs and compositions of major groups in Zhengzhou and other cities in China

	Guangzhou	Nanjing	Beijing	Hangzhou	Wuhan	Zhengzhou
Items	March-December, 2005	2011-2012	August, 2006	July-August, 2013	2013- 2014	May-September, 2017
Sampling site	residents-commercial -transportation mixed area	transportation- industry mixed area	residents- commercial mixed area	residents- transportation mixed area	urban	urban
Quantified compounds	59 NMHC	56 NMHC	47 NMHC	56 NMHC	99 VOCs	56 NMHC
Total samples	145	—	24	—	—	400
TNMHC (ppbv)	47.3	43.5	65.6±17.4	55.9	23.3±0.5	29.2±23.1
Compositions of major groups (%)	<i>alkane</i> 49.0 <i>alkene</i> 16 <i>aromatic</i> 23 <i>alkyne</i> 12	45.0 25.3 22.3 7.3	52.3 21.2 18.1 8.4	33.2 25.9 24.3 16.6		56.7±12.4 16.2±7.6 14.1±8.4 12.9±6.7
Reference	(Li and Wang, 2012)	(An et al., 2014)	(Guo et al., 2012)	(Li et al., 2017b)	(Lyu et al., 2016)	this study

558

559

560

561

562
563
564
565
566
567
568
569
570
571
572
573
574
575
576
577
578
579
580
581

Table 4. Specific information on VOCs, O₃ and NO at the four sites in June, 2017

Composition or conc.	JK	MEM	YH	GS
Aromatic (%)	9.06	11.6	4.72	15.8
Alkene (%)	6.36	4.13	5.52	5.47
Σ_{VOCs} (ppbv)	34.0	30.3	28.3	39.3
O ₃ (ppbv)	74.9	73.5	73.8	88.0
NO (ppbv)	7.10	7.72	2.34	4.47

582
583

Table 5. Top 10 VOCs ranked according to calculated ozone formation potential (OFP) and their corresponding percentage weighted in mixing ratio

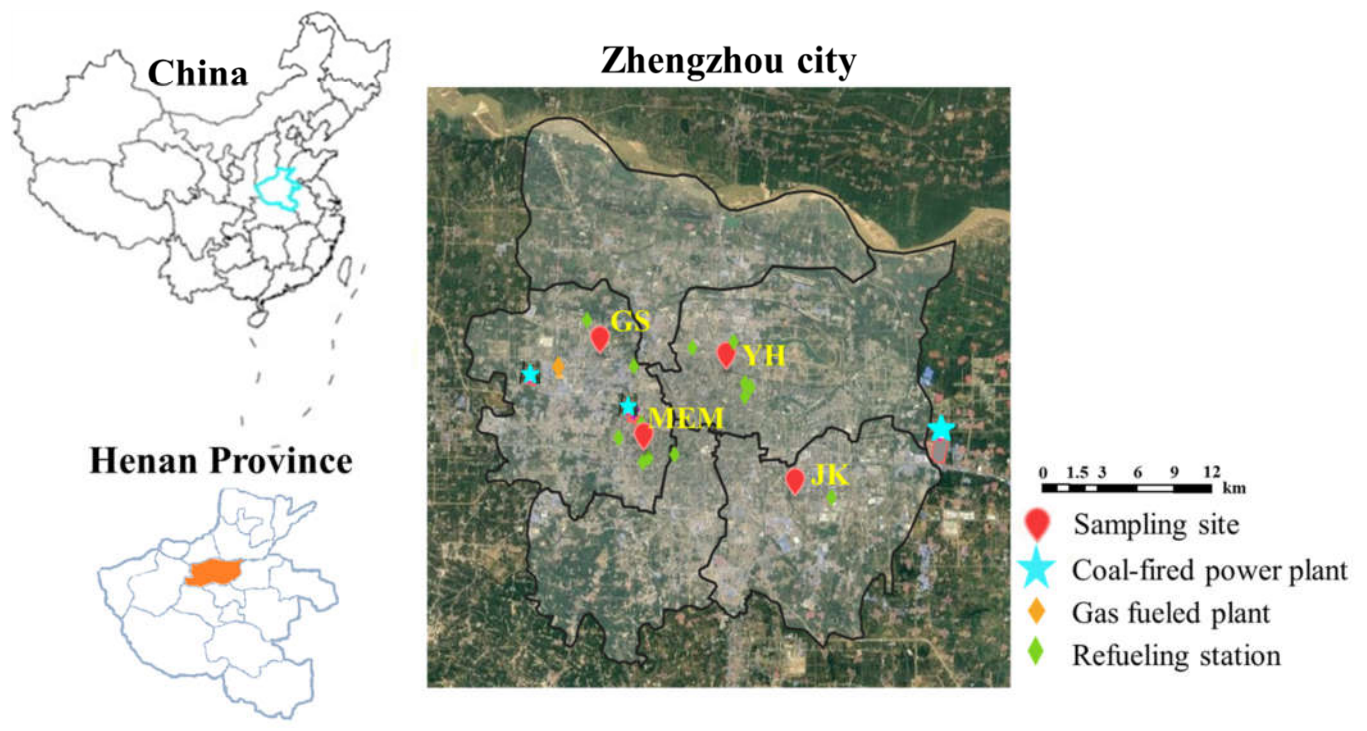
Site	Species	OFP (ppbv)	Weighted in OFP (%)	Weighted in mixing ratio (%)	Site	Species	OFP (ppbv)	Weighted in OFP (%)	Weighted in mixing ratio (%)
JK	Ethylene	19.0	25.5	8.22	MEM	Ethylene	18.4	30.9	7.92
	Isoprene	13.0	21.8	7.31		Isoprene	4.66	10.1	2.36
	m/p-Xylene	6.08	5.89	2.67		Toluene	3.73	6.67	3.99
	Toluene	5.53	5.83	4.22		Propylene	3.60	6.16	1.25
	Propylene	4.03	5.36	1.29		Acetylene	2.82	5.00	12.2
	Acetylene	2.97	4.44	13.5		m/p-Xylene	2.55	4.20	1.40
	n-Butane	2.15	3.05	7.28		n-Butane	1.81	3.20	5.97
	o-Xylene	1.83	2.00	0.88		Isopentane	1.76	3.16	7.39
	Isopentane	1.66	1.95	6.50		Ethane	1.58	2.96	23.4
	Propane	1.17	1.73	9.77		Propane	1.31	2.48	10.6
YH	Ethylene	19.8	28.1	8.88	GS	Ethylene	18.1	26.90	7.51
	Isoprene	7.44	11.3	3.67		Isoprene	8.01	16.8	4.64
	Toluene	6.63	7.75	5.72		Toluene	7.43	7.67	5.49
	m/p-Xylene	3.93	4.38	1.58		Propylene	4.39	5.85	1.26
	Acetylene	3.15	4.38	13.9		m/p-Xylene	4.31	4.57	1.75
	Propylene	3.01	3.60	0.91		Acetylene	2.76	4.24	12.1
	Trans-2-pentene	2.25	2.94	3.43		n-Butane	1.82	2.93	6.39
	n-Butane	1.84	2.80	6.31		Isopentane	1.71	2.68	6.94
	Isopentane	1.59	2.22	6.69		Propane	1.38	2.26	11.6
	Propane	1.18	1.98	10.2		Isobutane	1.13	1.98	4.59

584

^a *m*-Xylene and *p*-Xylene are co-eluted in the chromatographic separation.

585

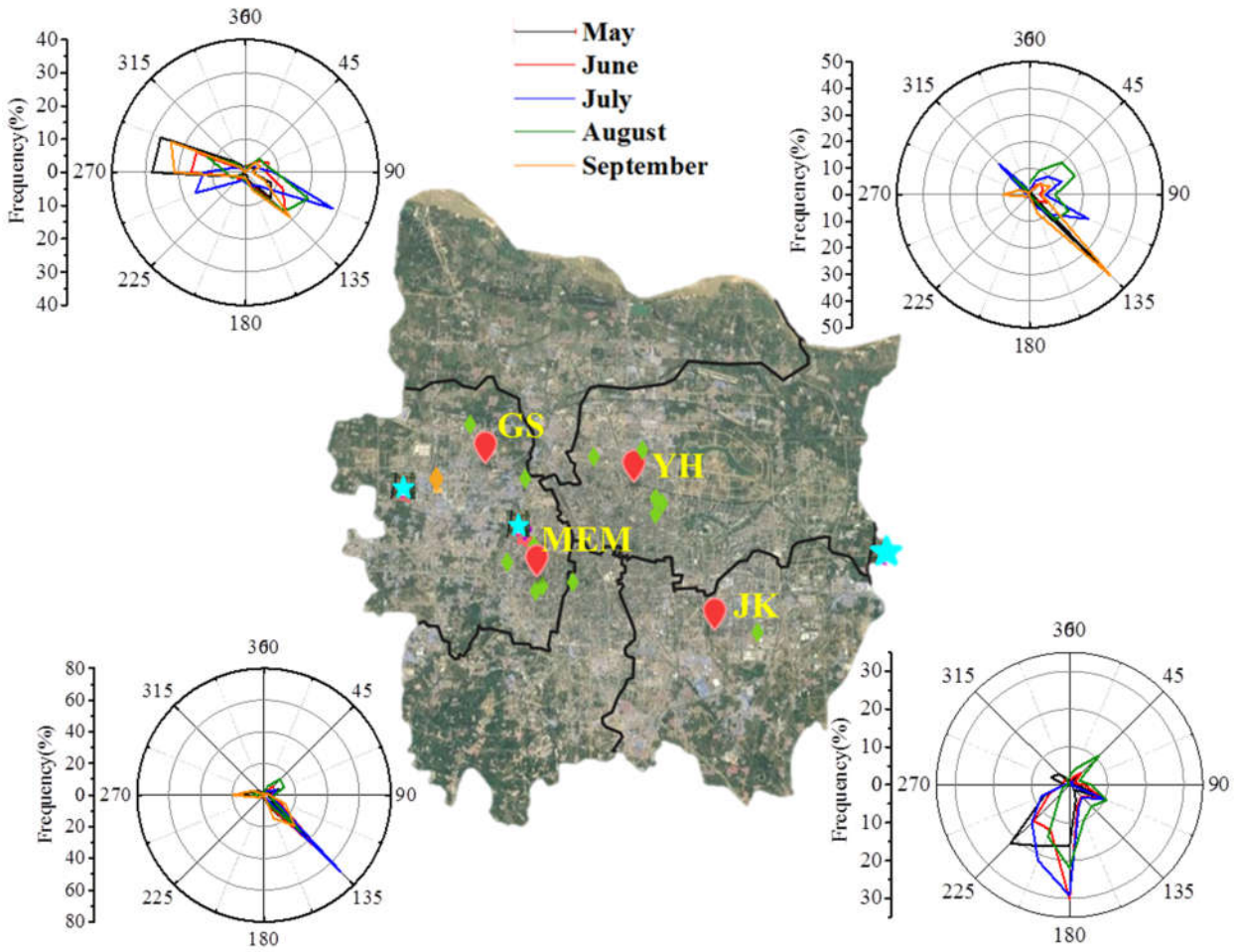
586



587

588 Fig. 1. Satellite imagery showing the four sampling sites and surrounding areas of Zhengzhou, China, including
589 major emission sources presented with different marks

590

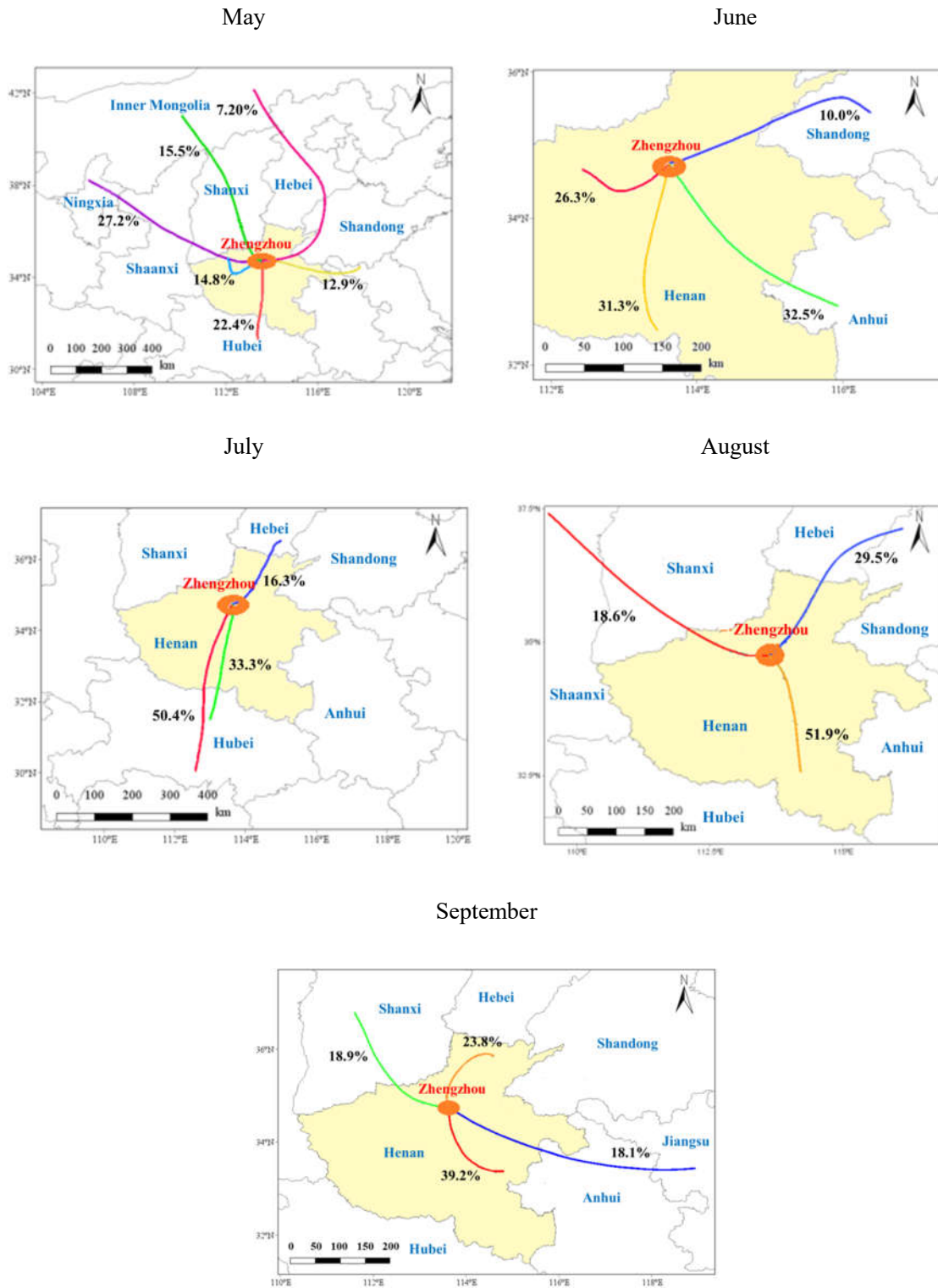


591

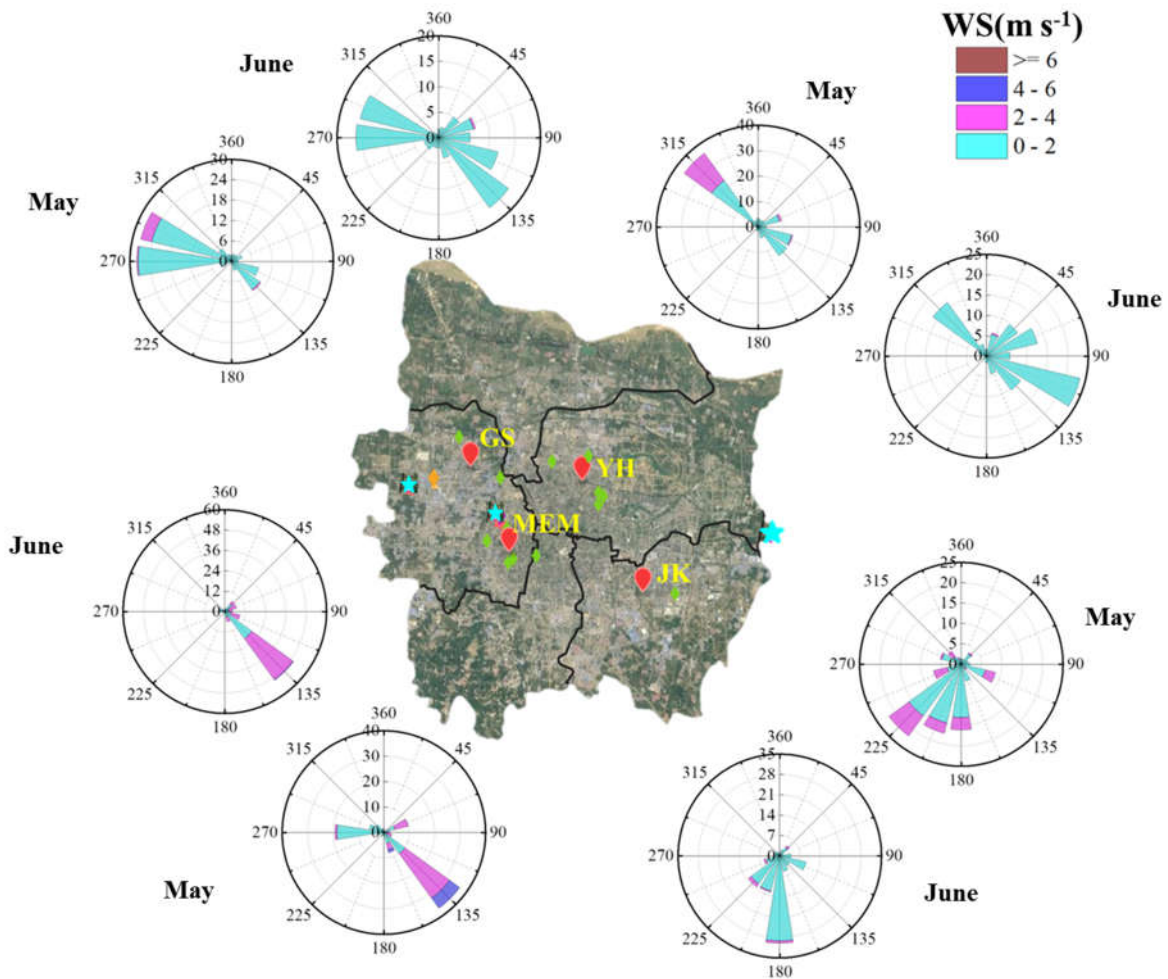
592

Fig. 2. Wind direction for each site during May to September, 2017

593



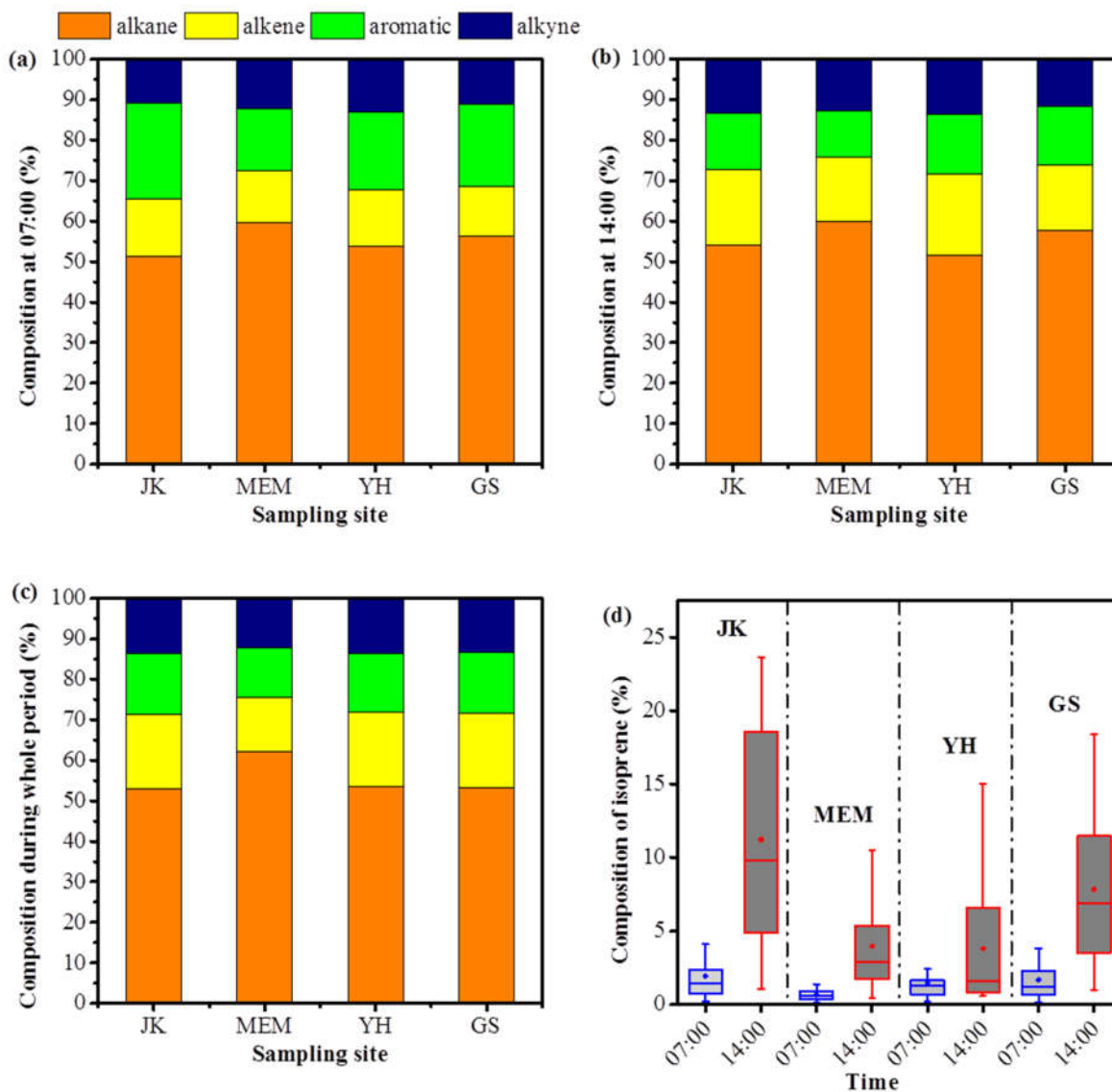
594 Fig. 3. Cluster analysis of 48-hour backward trajectories for Zhengzhou in each sampling month using HYSPLIT
 595 code, with the start height at 500m altitude and running interval set as 2- hour for each day, percentage of each
 596 cluster and covered areas are presented as well.



597

598 Fig. 4. Wind rose plot showing wind sector frequency (%) of occurrence and associated wind speed ($m s^{-1}$) at
 599 each site in May and June (the wind distribution in other three months were illustrated in Fig. S2), which were
 600 recorded by the anemometers placed at the same site with other air monitors.

601



603

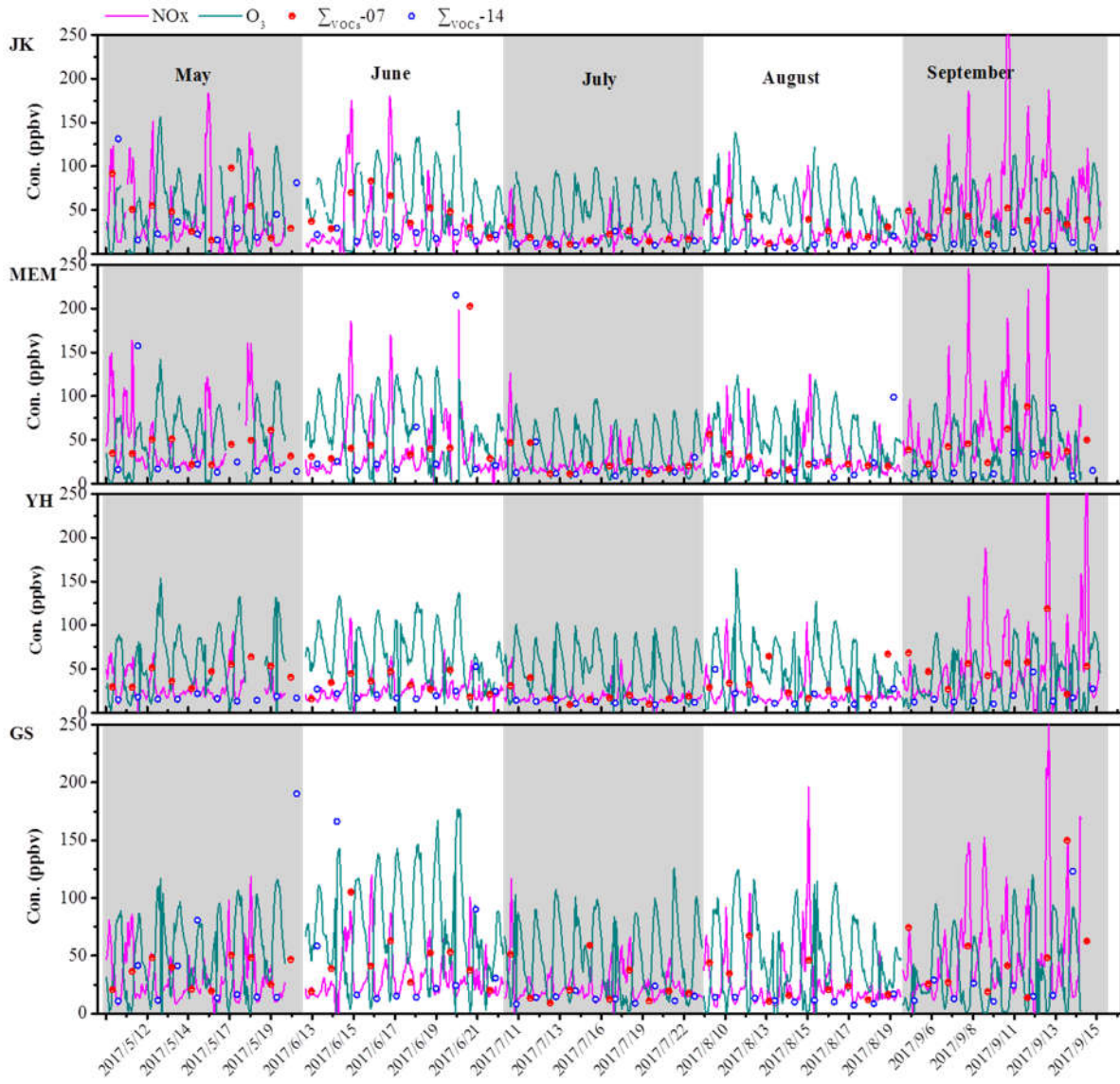
604 Fig. 5. Compositions of major organic classes at 07:00 LT (a), 14:00 LT (b) and during the whole sampling period

605 (c) at the four sites, and the box plot for the composition of isoprene at 07:00 LT and 14:00 LT for each site, with

606 the whiskers range in 5-95%iles, and the box shows the 25-75%iles, the solid dots represents the arithmetic

607 average, the line in the box shows the median (d).

608



610

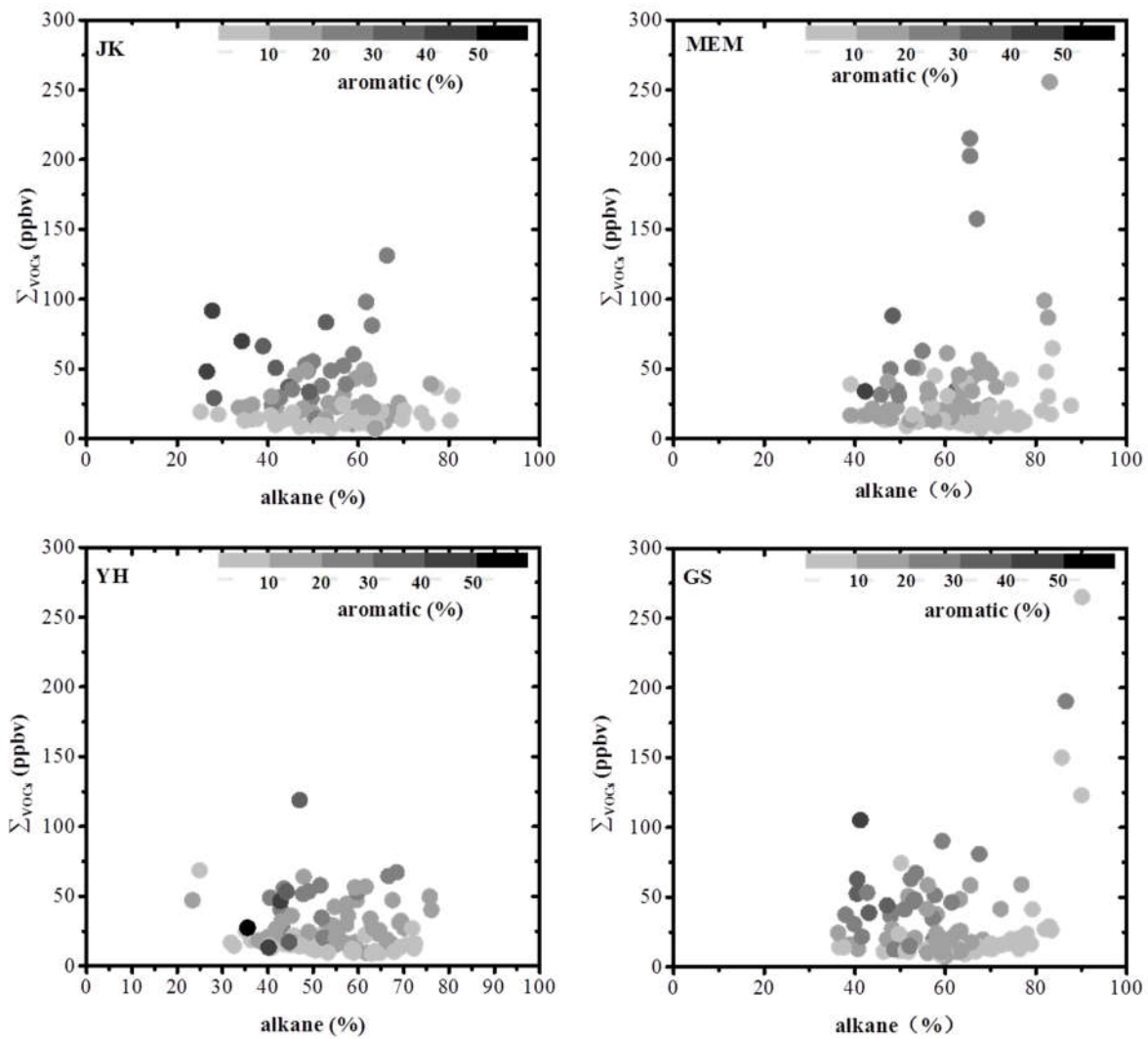
611 Fig. 6. Temporal variations of mixing ratios of ΣVOCs , NO_x and O_3 at the four sites during the whole sampling612 period, in which $\Sigma \text{VOCs-07}$ stands for the concentration level of ΣVOCs observed at 07:00 LT, and $\Sigma \text{VOCs-14}$

613

was that observed at 14:00 LT.

614

615

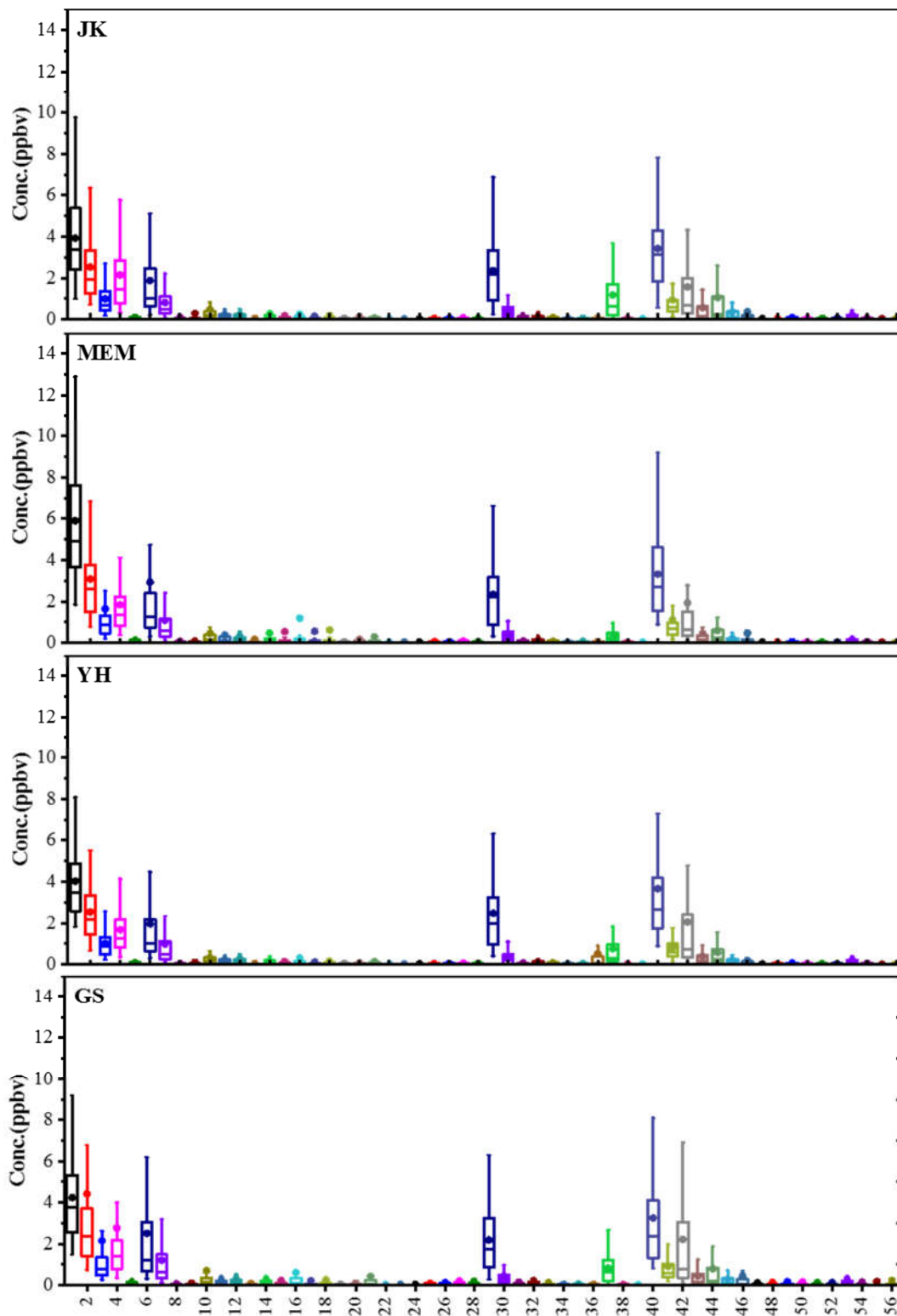


617

618 Fig. 7. The relationship between mixing ratio of Σ_{VOCs} and the composition of alkane, the data points are color

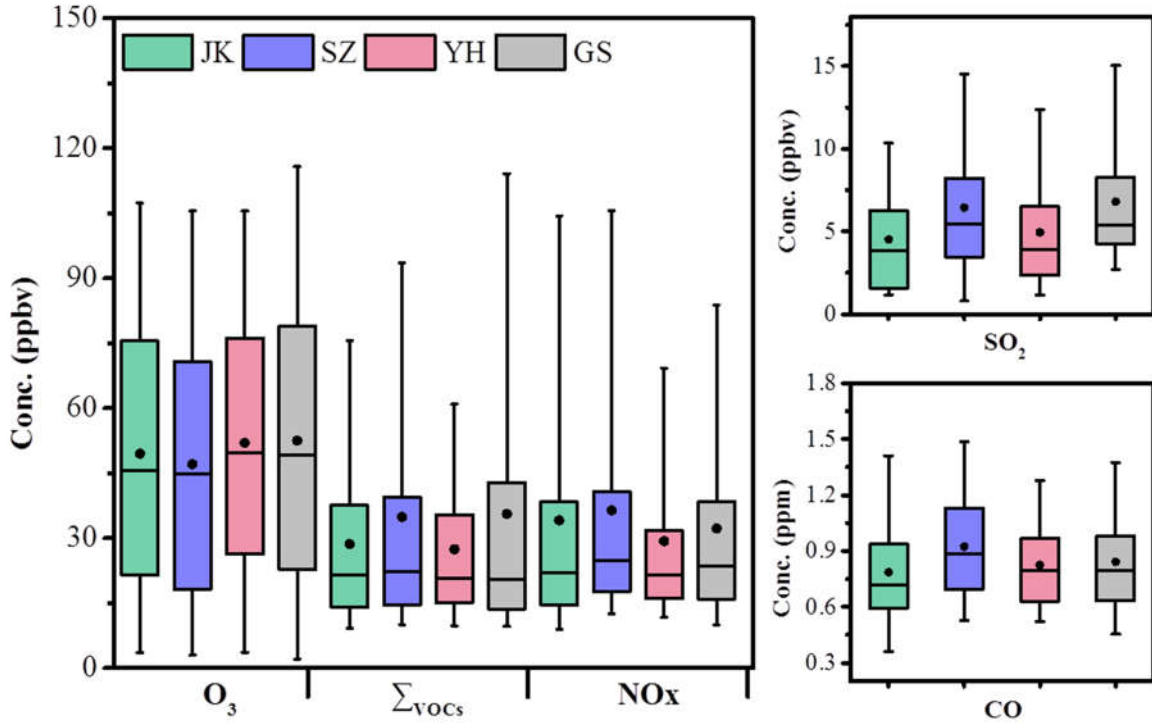
619 coded with the composition of aromatic.

620



621

622 Fig. 8. Concentrations of 57 VOCs at each site for the whole sampling period, the whiskers show the 5-95%iles,
 623 and the box shows the 25-75%iles, the solid points shows the arithmetic average, the line in the box shows the
 624 median. The chemicals are listed in Table S1.



625

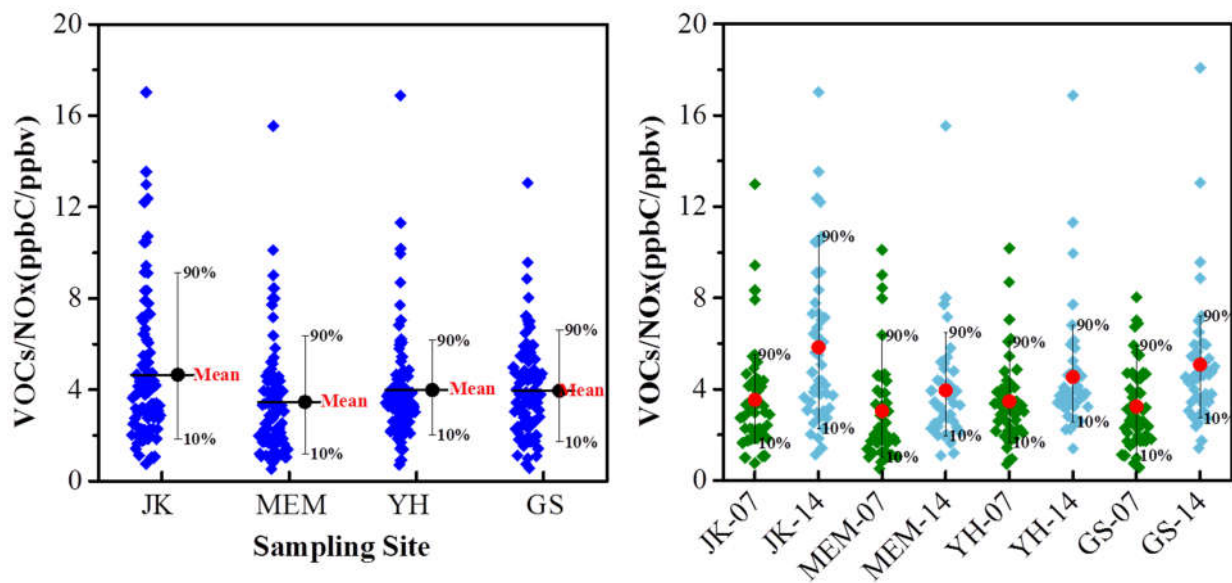
626

627

628

629

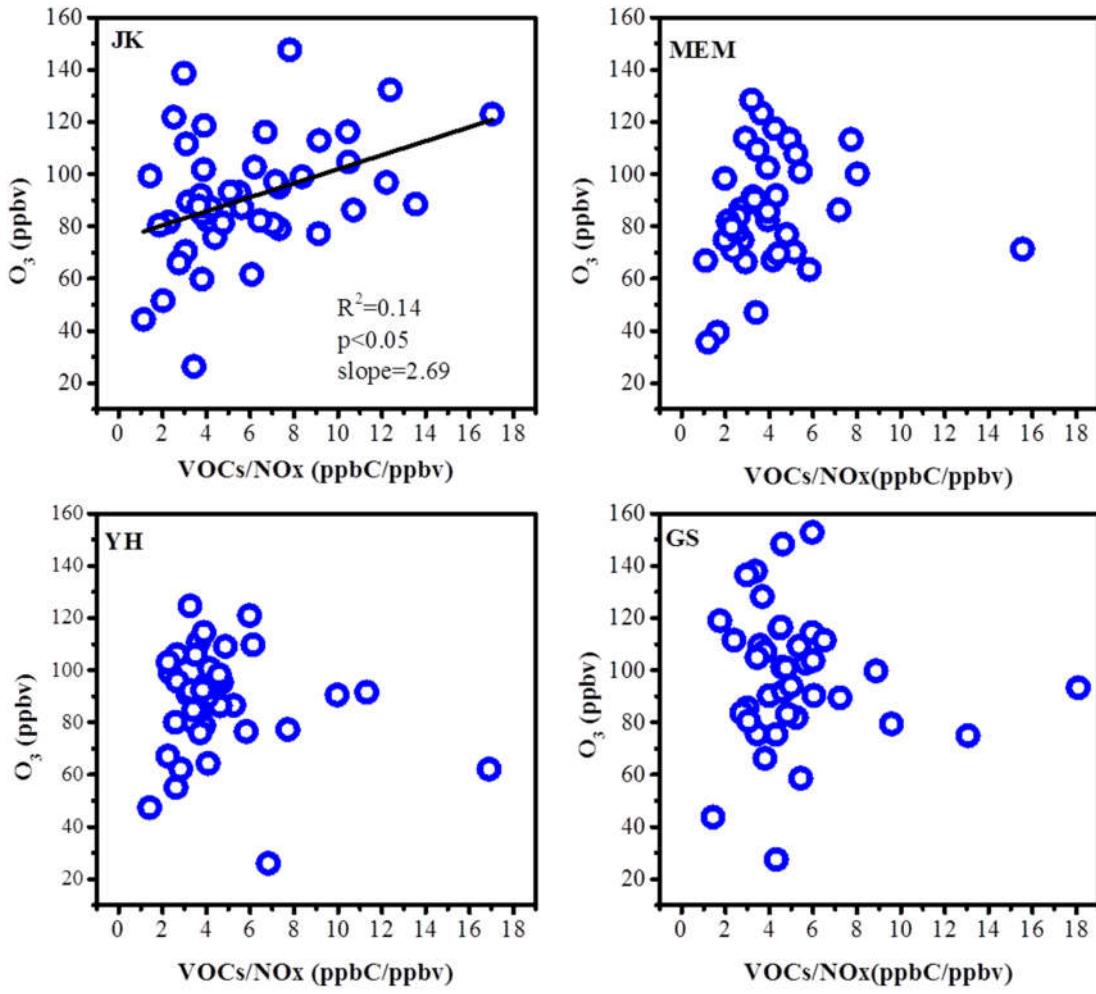
Fig. 9. The distribution of concentration point on O₃, ΣVOCs, NO_x, SO₂ and CO at each site, the range of the box was 25%-75%, the black line in the box stands for median level, the black dot represent the average level, the range of whisker was 5-95%.



630

631 Fig. 10. The data distribution of VOCs/NO_x(ppbC/ppbv) at the four sites (left), and the ratio observed at 07:00 LT
 632 and 14:00 LT were presented (right).

633



634

635

636

637

638

Fig. 11. The relationship between O₃ and VOCs/NO_x at 14:00 LT for each of the four sampling sites.

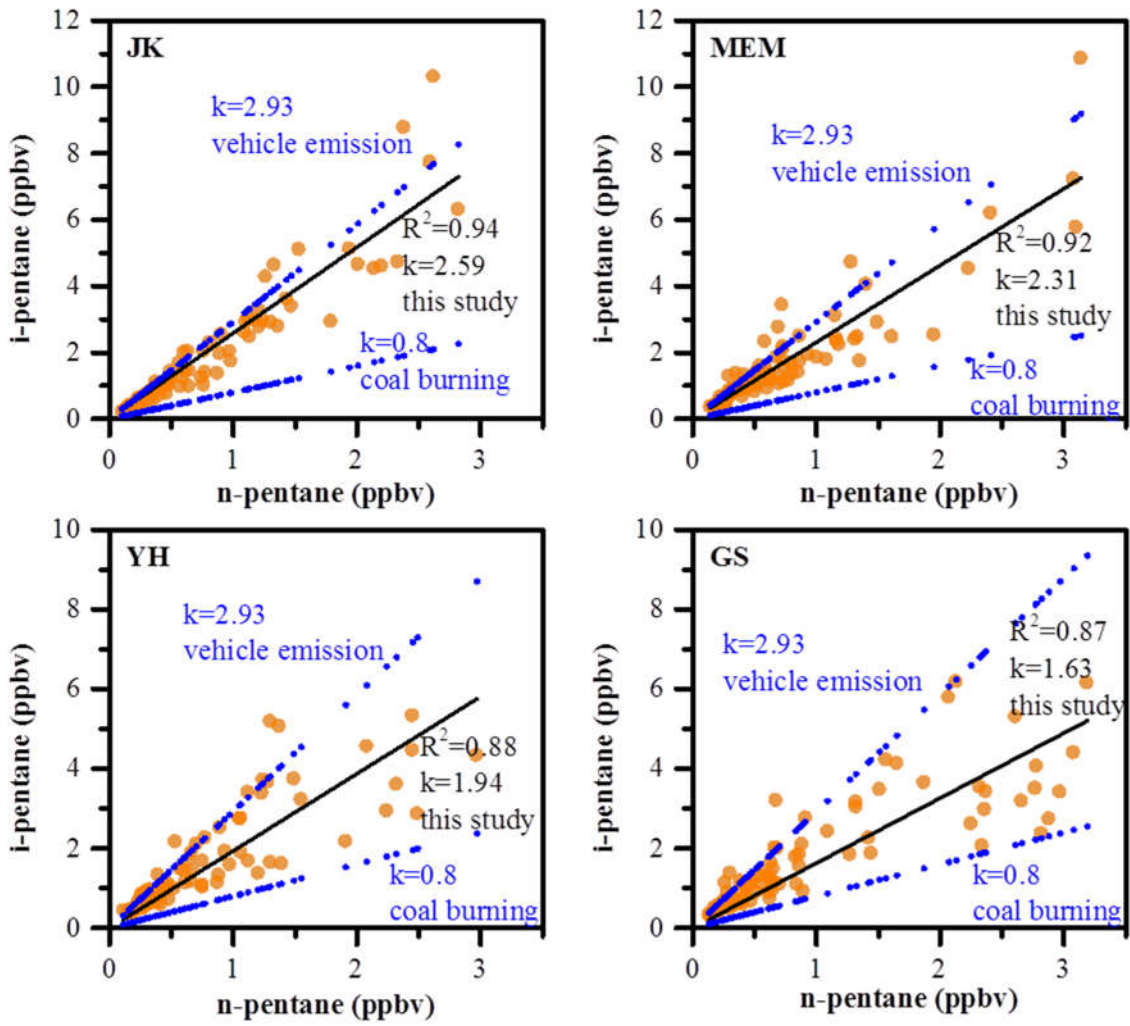


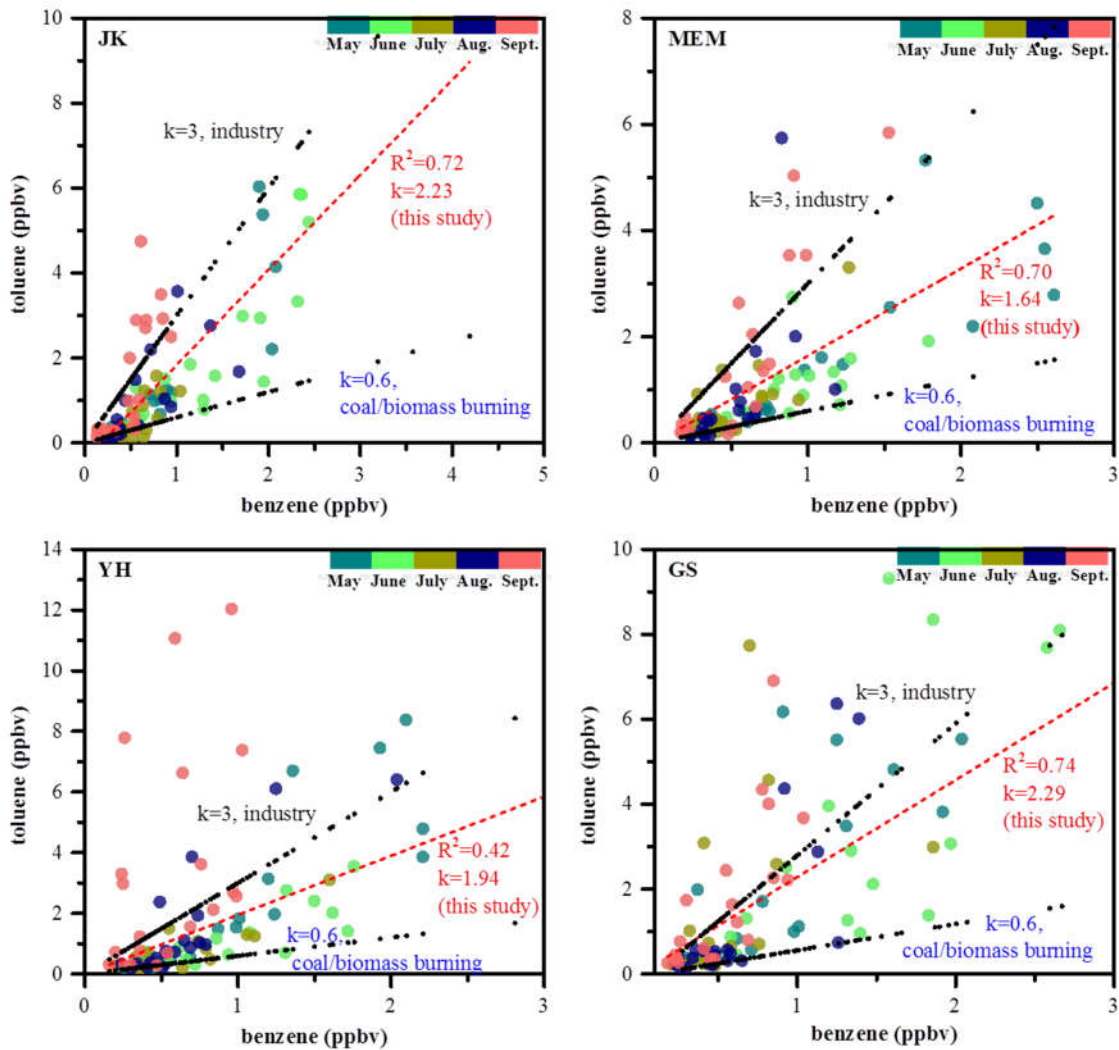
Fig. 12. Ratios of isopentane to n-pentane at every site

639

640

641

642



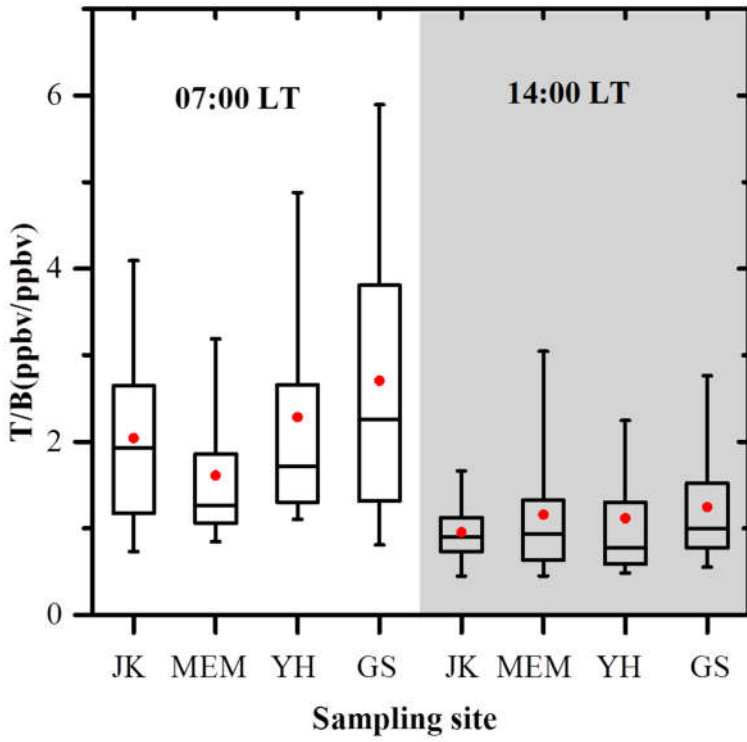
643

644 Fig. 13. T/B ratios and linear correlation coefficients (R^2) between benzene and toluene at every site, the data points
 645 were color mapped with sampling period.

646

647

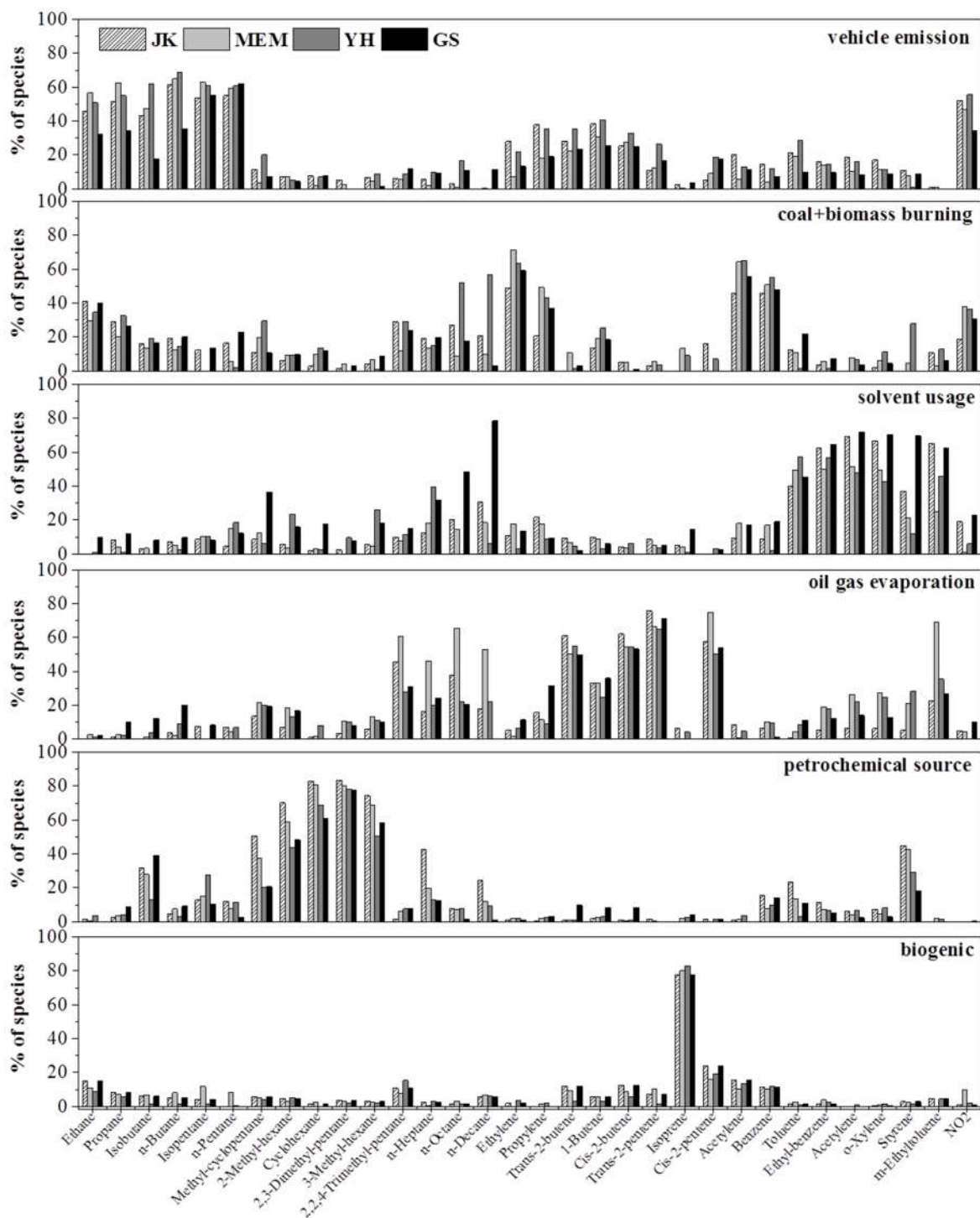
648



649

650 Fig. 14. The average ratio of T/B at 07:00LT and 14:00LT for each site during the whole sampling period

651



652

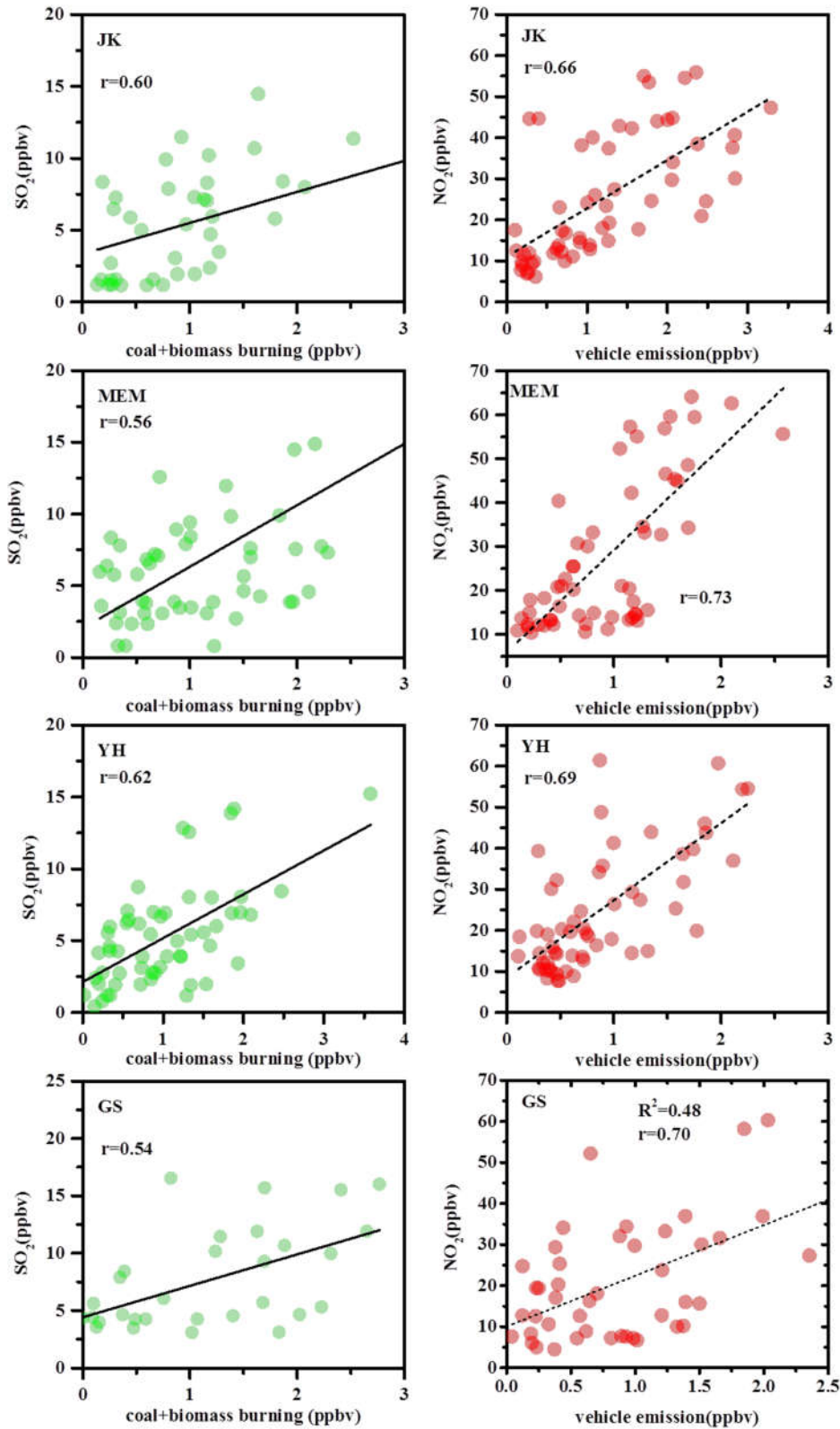
653

654

655

656

Fig. 15. Factor profiles of major emission sources, namely vehicle emission, coal+biomass burning, solvent usage, oil gas evaporation, petrochemical and biogenic source resolved by positive matrix factorization (PMF) model.

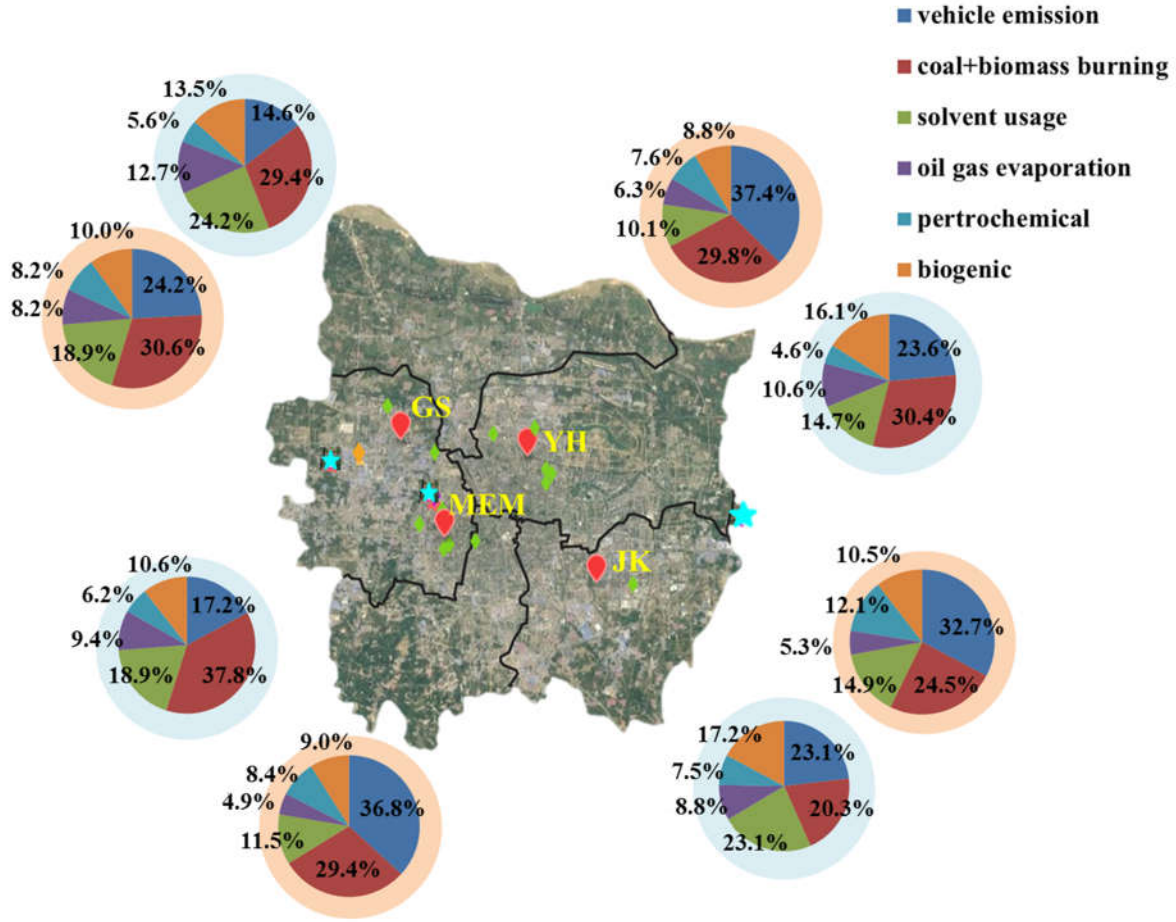


657

658

659

Fig. 16. Correlation analysis relating source-apportioned VOC contributions of coal+biomass burning (left column) and vehicle emission (right column) with co-located measurements of SO₂ and NO₂ for each site (rows).



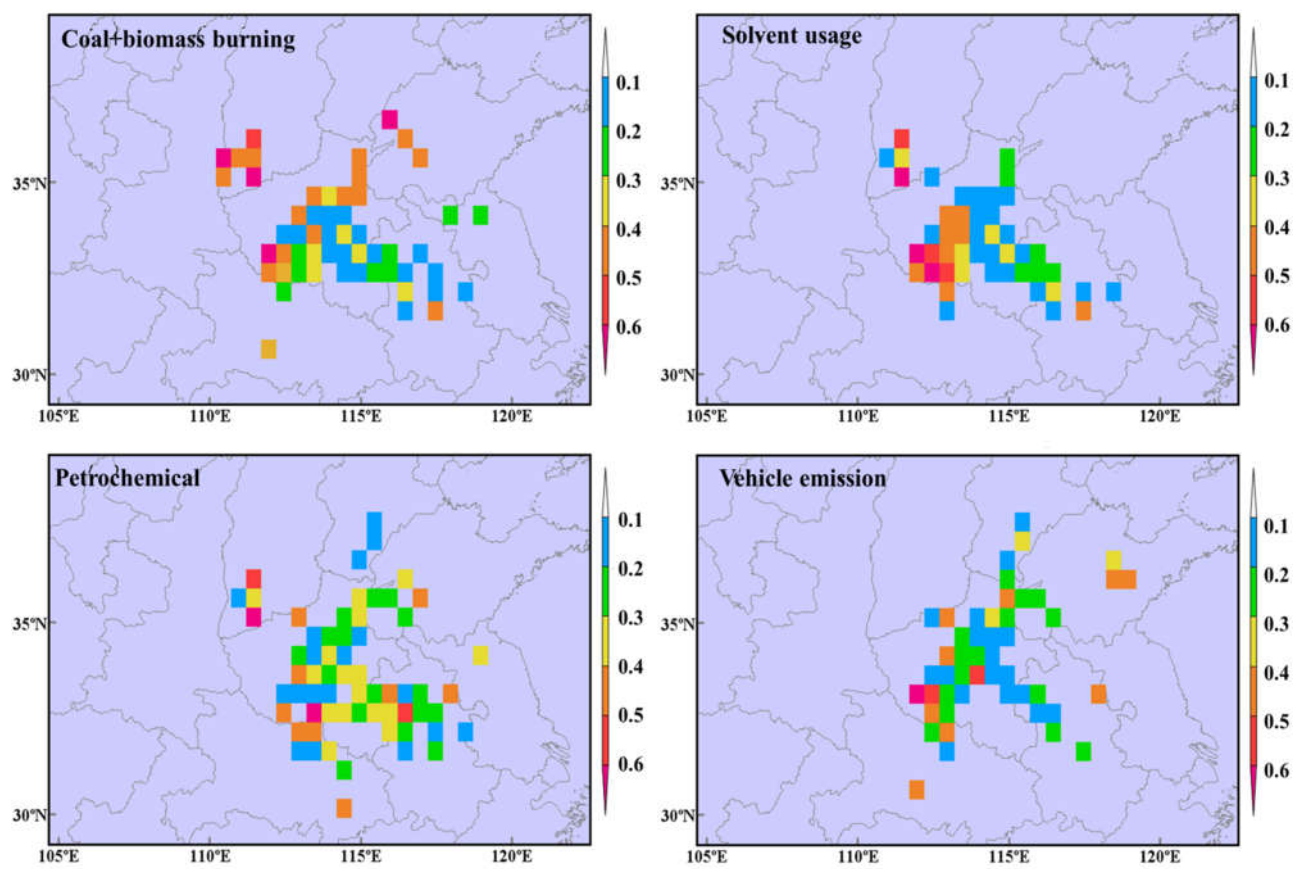
661

662 Fig. 17. Source apportionment results during the whole sampling period. The results weighted in observed
 663 concentrations were shadowed with pink color, and the results estimated based on OFP were shadowed with light
 664 blue color.

665

666

667



669

670 Fig. 18. Probable source regions apportioned by PSCF at Zhengzhou at summer (June-Aug. 2017) during
 671 sampling period

672

673

674

675 **Reference**

- 676 Abeleira, A., Pollack, I. B., Sive, B., Zhou, Y., Fischer, E. V., and Farmer, D. K.: Source
677 characterization of volatile organic compounds in the Colorado Northern Front Range Metropolitan
678 Area during spring and summer 2015, *J. Geophys. Res.-Atmos.*, 10.1002/2016jd026227, 2017.
- 679 Akagi, S. K., Yokelson, R. J., Wiedinmyer, C., Alvarado, M. J., Reid, J. S., Karl, T., Crouse, J. D.,
680 and Wennberg, P. O.: Emission factors for open and domestic biomass burning for use in
681 atmospheric models, *Atmos. Chem. Phys.*, 11, 4039-4072, 10.5194/acp-11-4039-2011, 2011.
- 682 An, J., Zhu, B., Wang, H., Li, Y., Lin, X., and Yang, H.: Characteristics and source apportionment
683 of VOCs measured in an industrial area of Nanjing, Yangtze River Delta, China, *Atmos. Environ.*,
684 97, 206-214, 10.1016/j.atmosenv.2014.08.021, 2014.
- 685 Barletta, B., Meinardi, S., Sherwood Rowland, F., Chan, C.-Y., Wang, X., Zou, S., Yin Chan, L.,
686 and Blake, D. R.: Volatile organic compounds in 43 Chinese cities, *Atmos. Environ.*, 39,
687 5979-5990, 10.1016/j.atmosenv.2005.06.029, 2005.
- 688 Borbon, A., Locoge, N., Veillerot, M., Galloo, J. C., and Guillermo, R.: Characterisation of
689 NMHCs in a French urban atmosphere: overview of the main sources, *Sci. Total Environ.*, 292
690 177–191, 2002.
- 691 Carter, W. P. L.: Development of Ozone Reactivity Scales for Volatile Organic Compounds, *J. Air
692 & Waste Manage. Assoc.*, 44, 881-899, 1994.
- 693 Carter, W. P. L.: Development of the SAPRC-07 Chemical Mechanism and Updated Ozone
694 Reactivity Scales, available at: <http://www.cert.ucr.edu/~carter/SAPRC>, (last access: 13 March,
695 2018), 2010.
- 696 Chen, W. T., Shao, M., Lu, S. H., Wang, M., Zeng, L. M., Yuan, B., and Liu, Y.: Understanding
697 primary and secondary sources of ambient carbonyl compounds in Beijing using the PMF model,
698 *Atmos. Chem. Phys.*, 14, 3047-3062, 10.5194/acp-14-3047-2014, 2014.
- 699 Cheng, L., Fu, L., Angle, R. P., and Sandhu, H. S.: Seasonal variations of volatile organic
700 compounds in Edmonton, Alberta, *Atmos. Environ.*, 31, 239-246, 1997.
- 701 Choek, D. P., and Heuss, J. M.: Urban ozone and its precursors, *Environ. Sci. Technol.*, 21,
702 1146-1153, 1987.

703 Chinese Ministry of Environmental Protection: Ambient Air Quality Index (AQI) Technical
704 Provisions (Trial), available at:
705 http://kjs.mee.gov.cn/hjbhzbz/bzwb/jcffbz/201203/t20120302_224166.shtml, (last access: 03
706 November, 2018), 2012.

707 Duan, J., Tan, J., Yang, L., Wu, S., and Hao, J.: Concentration, sources and ozone formation
708 potential of volatile organic compounds (VOCs) during ozone episode in Beijing, *Atmos. Res.*, 88,
709 25-35, 10.1016/j.atmosres.2007.09.004, 2008.

710 Fujita, E. M., Watson, J. G., Chow, J. C., and Lu, Z.: Validation of the chemical mass balance
711 receptor model applied to hydrocarbon source apportionment in the southern California air quality
712 study, *Environ. Sci. Technol.*, 28, 1633-1649, 1994.

713 Fujita, E. M.: Hydrocarbon source apportionment for the 1996 Paso del Norte Ozone Study, *Sci.*
714 *Total Environ.*, 276, 171-184, 2001.

715 Gao, W., Tie, X., Xu, J., Huang, R., Mao, X., Zhou, G., and Chang, L.: Long-term trend of O₃ in a
716 mega City (Shanghai), China: Characteristics, causes, and interactions with precursors, *Sci. Total*
717 *Environ.*, 603-604, 425-433, 10.1016/j.scitotenv.2017.06.099, 2017.

718 Geng, N., Wang, J., Xu, Y., Zhang, W., Chen, C., and Zhang, R.: PM_{2.5} in an industrial district of
719 Zhengzhou, China: Chemical composition and source apportionment, *Particuology*, 11, 99-109,
720 10.1016/j.partic.2012.08.004, 2013.

721 Gentner, D. R., Worton, D. R., Isaacman, G., Davis, L. C., Dallmann, T. R., Wood, E. C., Herndon,
722 S. C., Goldstein, A. H., and Harley, R. A.: Chemical composition of gas-phase organic carbon
723 emissions from motor vehicles and implications for ozone production, *Environ. Sci. Technol.*, 47,
724 11837-11848, 10.1021/es401470e, 2013.

725 Gilman, J. B., Lerner, B. M., Kuster, W. C., and de Gouw, J. A.: Source signature of volatile
726 organic compounds from oil and natural gas operations in northeastern Colorado, *Environ. Sci.*
727 *Technol.*, 47, 1297-1305, 10.1021/es304119a, 2013.

728 Gong, M., Yin, S., Gu, X., Xu, Y., Jiang, N., and Zhang, R.: Refined 2013-based vehicle emission
729 inventory and its spatial and temporal characteristics in Zhengzhou, China, *Sci. Total Environ.*,
730 599-600, 1149-1159, 10.1016/j.scitotenv.2017.03.299, 2017.

731 Guenther, A., Hewitt, C. N., Erickson, D., Fall, R., Geron, C., Graedel, T., Harley, P., Klinger, L.,
732 Lerda, M., McKay, W. A., Pierce, T., Scholes, B., Steinbrecher, R., Tallamraju, R., Taylor, J., and
733 Zimmerman, P.: A global model of natural volatile organic compound emissions, *J. Geophys. Res.*,
734 100, 8873-8892, 1995.

735 Guenther, A. B., Zimmerman, P. R., and Harley, P. C.: Isoprene and monoterpene emission rate
736 variability: model evaluations and sensitivity analyses, *J. Geophys. Res.*, 98, 12,609-612,617, 1993.

737 Guo, H., Cheng, H. R., Ling, Z. H., Louie, P. K., and Ayoko, G. A.: Which emission sources are
738 responsible for the volatile organic compounds in the atmosphere of Pearl River Delta?, *J. Hazard.*
739 *Mater.*, 188, 116-124, 10.1016/j.jhazmat.2011.01.081, 2011.

740 Guo, H., Ling, Z. H., Cheng, H. R., Simpson, I. J., Lyu, X. P., Wang, X. M., Shao, M., Lu, H. X.,
741 Ayoko, G., Zhang, Y. L., Saunders, S. M., Lam, S. H. M., Wang, J. L., and Blake, D. R.:
742 Tropospheric volatile organic compounds in China, *Sci. Total Environ.*, 574, 1021-1043,
743 10.1016/j.scitotenv.2016.09.116, 2017.

744 Guo, S., Tan, J., Duan, J., Ma, Y., Yang, F., He, K., and Hao, J.: Characteristics of atmospheric
745 non-methane hydrocarbons during haze episode in Beijing, China, *Environ. Monit. Assess.*, 184,
746 7235-7246, 10.1007/s10661-011-2493-9, 2012.

747 Haagen-Smit, A. T.: Chemistry and physiology of Los Angeles smog, *J. Ind. Eng. Chem.*, 44,
748 1342-1346, 1952.

749 Hanna, S. R., Moore, G. E., and Fernau, M.: Evaluation of photochemical grid models (UAM-IV,
750 UAM-V, and the ROM/UAM-IV couple) using data from the Lake Michigan Ozone Study (LMOS)
751 *Atmos. Environ.*, 30, 3265-3279, 1996.

752 Hidy, G. M., and Blanchard, C. L.: Precursor reductions and ground-level ozone in the Continental
753 United States, *J. Air & Waste Manage. Assoc.*, 65, 1261-1282, 10.1080/10962247.2015.1079564,
754 2015.

755 Ho, K. F., Lee, S. C., Ho, W. K., Blake, D. R., Cheng, Y., Li, Y. S., Ho, S. S. H., Fung, K., Louie, P.
756 K. K., and Park, D.: Vehicular emission of volatile organic compounds (VOCs) from a tunnel study
757 in Hong Kong, *Atmos. Chem. Phys.*, 9, 7491-7504, 2009.

758 Hopke, P. K., Barrie, L. A., Li, S.-M., M.-D.Cheng, C.Li, and Xie, Y.: Possible sources and
759 preferred pathways for biogenic and non-sea-salt sulfur for the high Arctic, *J. Geophys.*
760 *Res.-Atmos.*, 100, 16,595-516,603, 1995.

761 Huang, Y., Ling, Z. H., Lee, S. C., Ho, S. S. H., Cao, J. J., Blake, D. R., Cheng, Y., Lai, S. C., Ho,
762 K. F., Gao, Y., Cui, L., and Louie, P. K. K.: Characterization of volatile organic compounds at a
763 roadside environment in Hong Kong: An investigation of influences after air pollution control
764 strategies, *Atmos. Environ.*, 122, 809-818, 10.1016/j.atmosenv.2015.09.036, 2015.

765 Jia, C., Mao, X., Huang, T., Liang, X., Wang, Y., Shen, Y., Jiang, W., Wang, H., Bai, Z., Ma, M.,
766 Yu, Z., Ma, J., and Gao, H.: Non-methane hydrocarbons (NMHCs) and their contribution to ozone
767 formation potential in a petrochemical industrialized city, Northwest China, *Atmos. Res.*, 169,
768 225-236, 10.1016/j.atmosres.2015.10.006, 2016.

769 Jin, X., and Holloway, T.: Spatial and temporal variability of ozone sensitivity over China observed
770 from the Ozone Monitoring Instrument, *J. Geophys. Res.-Atmos.*, 120, 7229-7246,
771 10.1002/2015jd023250, 2015.

772 Jobson, B. T., Berkowitz, C. M., Kuster, W. C., Goldan, P. D., Williams, E. J., Fesenfeld, F. C.,
773 Apel, E. C., Karl, T., Lonneman, W. A., and Riemer, D.: Hydrocarbon source signatures in Houston,
774 Texas: Influence of the petrochemical industry, *J. Geophys. Res.-Atmos.*, 109,
775 10.1029/2004jd004887, 2004.

776 Lau, A. K., Yuan, Z., Yu, J. Z., and Louie, P. K.: Source apportionment of ambient volatile organic
777 compounds in Hong Kong, *Sci. Total Environ.*, 408, 4138-4149, 10.1016/j.scitotenv.2010.05.025,
778 2010.

779 Li, B., Ho, S. S. H., Xue, Y., Huang, Y., Wang, L., Cheng, Y., Dai, W., Zhong, H., Cao, J., and Lee,
780 S.: Characterizations of volatile organic compounds (VOCs) from vehicular emissions at roadside
781 environment: The first comprehensive study in Northwestern China, *Atmos. Environ.*, 161, 1-12,
782 10.1016/j.atmosenv.2017.04.029, 2017a.

783 Li, K., Chen, L., Ying, F., White, S. J., Jang, C., Wu, X., Gao, X., Hong, S., Shen, J., Azzi, M., and
784 Cen, K.: Meteorological and chemical impacts on ozone formation: A case study in Hangzhou,
785 China, *Atmos. Res.*, 10.1016/j.atmosres.2017.06.003, 2017b.

786 Li, L., and Wang, X.: Seasonal and diurnal variations of atmospheric non-methane hydrocarbons in
787 Guangzhou, China, *Inter. J. .Env. Res. Pub. Heal.*, 9, 1859-1873, 10.3390/ijerph9051859, 2012.

788 Li, L., Chen, Y., Zeng, L., Shao, M., Xie, S., Chen, W., Lu, S., Wu, Y., and Cao, W.: Biomass
789 burning contribution to ambient volatile organic compounds (VOCs) in the Chengdu–Chongqing
790 Region (CCR), China, *Atmos. Environ.*, 99, 403-410, 10.1016/j.atmosenv.2014.09.067, 2014.

791 Li, Q., Zhang, L., Wang, T., Wang, Z., Fu, X., and Zhang, Q.: "New" Reactive Nitrogen Chemistry
792 Reshapes the Relationship of Ozone to Its Precursors, *Environ. Sci. Technol.*, 52, 2810-2818,
793 10.1021/acs.est.7b05771, 2018.

794 Lin, X., Traner, M., and Liu, S. C.: On the Nonlinearity of the Tropospheric Ozone Production, *J.*
795 *Geophys. Res.-Atmos.*, 93, 15879-15888, 1998.

796 Liu, B., Liang, D., Yang, J., Dai, Q., Bi, X., Feng, Y., Yuan, J., Xiao, Z., Zhang, Y., and Xu, H.:
797 Characterization and source apportionment of volatile organic compounds based on 1-year of
798 observational data in Tianjin, China, *Environ. Pollut.*, 218, 757-769, 10.1016/j.envpol.2016.07.072,
799 2016.

800 Liu, H., Liu, S., Xue, B., Lv, Z., Meng, Z., Yang, X., Xue, T., Yu, Q., and He, K.: Ground-level
801 ozone pollution and its health impacts in China, *Atmos. Environ.*, 173, 223-230,
802 10.1016/j.atmosenv.2017.11.014, 2018.

803 Liu, Y., Shao, M., Fu, L., Lu, S., Zeng, L., and Tang, D.: Source profiles of volatile organic
804 compounds (VOCs) measured in China: Part I, *Atmos. Environ.*, 42, 6247-6260,
805 10.1016/j.atmosenv.2008.01.070, 2008.

806 Liu, Y., Yuan, B., Li, X., Shao, M., Lu, S., Li, Y., Chang, C. C., Wang, Z., Hu, W., Huang, X., He,
807 L., Zeng, L., Hu, M., and Zhu, T.: Impact of pollution controls in Beijing on atmospheric
808 oxygenated volatile organic compounds (OVOCs) during the 2008 Olympic Games: observation
809 and modeling implications, *Atmos. Chem. Phys.*, 15, 3045-3062, 10.5194/acp-15-3045-2015, 2015.

810 Louie, P. K. K., Ho, J. W. K., Tsang, R. C. W., Blake, D. R., Lau, A. K. H., Yu, J. Z., Yuan, Z.,
811 Wang, X., Shao, M., and Zhong, L.: VOCs and OVOCs distribution and control policy implications
812 in Pearl River Delta region, China, *Atmos. Environ.*, 76, 125-135, 10.1016/j.atmosenv.2012.08.058,
813 2013.

814 Luecken, D. J., Napelenok, S. L., Strum, M., Scheffe, R., and Phillips, S.: Sensitivity of Ambient
815 Atmospheric Formaldehyde and Ozone to Precursor Species and Source Types Across the United
816 States, *Environ. Sci. Technol.*, 52, 4668-4675, 10.1021/acs.est.7b05509, 2018.

817 Lyu, X. P., Chen, N., Guo, H., Zhang, W. H., Wang, N., Wang, Y., and Liu, M.: Ambient volatile
818 organic compounds and their effect on ozone production in Wuhan, central China, *Sci. Total
819 Environ.*, 541, 200-209, 10.1016/j.scitotenv.2015.09.093, 2016.

820 Malley, C. S., Braban, C. F., Dumitrean, P., Cape, J. N., and Heal, M. R.: The impact of speciated
821 VOCs on regional ozone increment derived from measurements at the UK EMEP supersites
822 between 1999 and 2012, *Atmos. Chem. Phys.*, 15, 8361-8380, 10.5194/acp-15-8361-2015, 2015.

823 McGaughey, G. R., Desai, N. R., Allen, D. T., Seila, R. L., Lonneman, W. A., Fraser, M. P., Harley,
824 R. A., Pollack, A. K., Ivy, J. M., and Price, J. H.: Analysis of motor vehicle emissions in a Houston
825 tunnel during the Texas Air Quality Study 2000, *Atmos. Environ.*, 38, 3363-3372,
826 10.1016/j.atmosenv.2004.03.006, 2004.

827 Na, K., Kim, Y. P., Moon, K.-C., Moon, I., and Fung, K.: Concentrations of volatile organic
828 compounds in an industrial area of Korea, *Atmos. Environ.*, 35, 2747-2756, 2001.

829 Nagashima, T., Sudo, K., Akimoto, H., Kurokawa, J., and Ohara, T.: Long-term change in the
830 source contribution to surface ozone over Japan, *Atmos. Chem. Phys.*, 17, 8231-8246,
831 10.5194/acp-17-8231-2017, 2017.

832 Oliver, K. D., Adams, J. R., JR, E. H. D., Mcclenny, W. A., Yoong, M. J., and Pardee, M. A.:
833 Technique for monitoring ozone precursor hydrocarbons in air at photochemical assessment
834 monitoring stations: sorbent preconcentration, closed-cycle cooler cryofocusing, and GC-FID
835 analysis, *Atmos. Environ.*, 30, 2751-2757, 1996.

836 Ou, J., Zheng, J., Li, R., Huang, X., Zhong, Z., Zhong, L., and Lin, H.: Speciated OVOC and VOC
837 emission inventories and their implications for reactivity-based ozone control strategy in the Pearl
838 River Delta region, China, *Sci. Total Environ.*, 530-531, 393-402, 10.1016/j.scitotenv.2015.05.062,
839 2015.

840 Ou, J., Yuan, Z., Zheng, J., Huang, Z., Shao, M., Li, Z., Huang, X., Guo, H., and Louie, P. K.:
841 Ambient Ozone Control in a Photochemically Active Region: Short-Term Despiking or Long-Term
842 Attainment?, *Environ. Sci. Technol.*, 50, 5720-5728, 10.1021/acs.est.6b00345, 2016.

843 Polissar, A. V., Hopke, P. K., Paatero, P., Kaufmann, Y. J., Hall, D. K., Bodhaine, B. A., Dutton, E.
844 G., and Harris, J. M.: The aerosol at Barrow, Alaska: long-term trends and source locations, *Atmos.*
845 *Environ.*, 33, 2441-2458, 1999.

846 Pollack, I. B., Ryerson, T. B., Trainer, M., Neuman, J. A., Roberts, J. M., and Parrish, D. D.:
847 Trends in ozone, its precursors, and related secondary oxidation products in Los Angeles,
848 California: A synthesis of measurements from 1960 to 2010, *J. Geophys. Res.-Atmos.*, 118,
849 5893-5911, 10.1002/jgrd.50472, 2013.

850 Raysoni, A. U., Stock, T. H., Sarnat, J. A., Chavez, M. C., Sarnat, S. E., Montoya, T., Holguin, F.,
851 and Li, W. W.: Evaluation of VOC concentrations in indoor and outdoor microenvironments at
852 near-road schools, *Environ. Pollut.*, 231, 681-693, 10.1016/j.envpol.2017.08.065, 2017.

853 Russo, R. S., Zhou, Y., White, M. L., Mao, H., Talbot, R., and Sive, B. C.: Multi-year (2004–2008)
854 record of nonmethane hydrocarbons and halocarbons in New England: seasonal variations and
855 regional sources, *Atmos. Chem. Phys.*, 10, 4909-4929, 10.5194/acp-10-4909-2010, 2010.

856 Shao, M., Lu, S., Liu, Y., Xie, X., Chang, C., Huang, S., and Chen, Z.: Volatile organic compounds
857 measured in summer in Beijing and their role in ground-level ozone formation, *J. Geophys.*
858 *Res.-Atmos.*, 114, 10.1029/2008jd010863, 2009.

859 Shao, M., Wang, B., Lu, S., Yuan, B., and Wang, M.: Effects of Beijing Olympics Control
860 Measures on Reducing Reactive Hydrocarbon Species, *Environ. Sci. Technol.*, 45, 514-519, 2011.

861 Shao, P., An, J., Xin, J., Wu, F., Wang, J., Ji, D., and Wang, Y.: Source apportionment of VOCs
862 and the contribution to photochemical ozone formation during summer in the typical industrial area
863 in the Yangtze River Delta, China, *Atmos. Res.*, 176-177, 64-74, 10.1016/j.atmosres.2016.02.015,
864 2016.

865 Shen, F., Ge, X., Hu, J., Nie, D., Tian, L., and Chen, M.: Air pollution characteristics and health
866 risks in Henan Province, China, *Environ. Res.*, 156, 625-634, 10.1016/j.envres.2017.04.026, 2017.

867 Shiu, C.-J., Liu, S. C., Chang, C.-C., Chen, J.-P., Chou, C. C. K., Lin, C.-Y., and Young, C.-Y.:
868 Photochemical production of ozone and control strategy for Southern Taiwan, *Atmos. Environ.*, 41,
869 9324-9340, 10.1016/j.atmosenv.2007.09.014, 2007.

870 Sillman, S.: The relation between ozone, NO_x and hydrocarbons in urban and polluted rural
871 environments, *Atmos. Environ.*, 33, 1821-1845, 1999.

872 Streets, D. G., Fu, J. S., Jang, C. J., Hao, J., He, K., Tang, X., Zhang, Y., Wang, Z., Li, Z., Zhang,
873 Q., Wang, L., Wang, B., and Yu, C.: Air quality during the 2008 Beijing Olympic Games, *Atmos.*
874 *Environ.*, 41, 480-492, 10.1016/j.atmosenv.2006.08.046, 2007.

875 Sun, J., Wu, F., Hu, B., Tang, G., Zhang, J., and Wang, Y.: VOC characteristics, emissions and
876 contributions to SOA formation during hazy episodes, *Atmos. Environ.*, 141, 560-570,
877 10.1016/j.atmosenv.2016.06.060, 2016.

878 Tang, J. H., Chan, L. Y., Chan, C. Y., Li, Y. S., Chang, C. C., Liu, S. C., Wu, D., and Li, Y. D.:
879 Characteristics and diurnal variations of NMHCs at urban, suburban, and rural sites in the Pearl
880 River Delta and a remote site in South China, *Atmos. Environ.*, 41, 8620-8632,
881 10.1016/j.atmosenv.2007.07.029, 2007.

882 Tsai, S. M., Zhang, J. J., Smith, K. R., Ma, Y., Rasmussen, R. A., and Khalil, M. A. K.:
883 Characterization of Non-methane Hydrocarbons Emitted from Various Cookstoves Used in China,
884 *Environ. Sci. Technol.*, 37, 2869-2877, 2003.

885 US EPA: Compendium Method TO-15: Determination of volatile organic compounds in air
886 collected in specially prepared canisters and analyzed by gas chromatography/mass spectrometry,
887 1999.

888 US EPA, National air pollutant emission trends 1900–1998, Off. Air Qual. Plann. Stand., Research
889 Triangle Park, N. C, Rep. EPA 454/R-00-002, 2000.

890 US EPA: Photochemical Assessment Monitoring Stations (PAMS), available at:
891 <https://www3.epa.gov/ttnamti1/pamsmain.html>, (last access: 03 December 2018), 1990.

892 Wang, H.-l., Jing, S.-a., Lou, S.-r., Hu, Q.-y., Li, L., Tao, S.-k., Huang, C., Qiao, L.-p., and Chen,
893 C.-h.: Volatile organic compounds (VOCs) source profiles of on-road vehicle emissions in China,
894 *Sci. Total Environ.*, 607-608, 253-261, 10.1016/j.scitotenv.2017.07.001, 2017a.

895 Wang, H., Qiao, Y., Chen, C., Lu, J., Qiao, L., and Lou, S.: Source Profiles and Chemical
896 Reactivity of Volatile Organic Compounds from Solvent Use in Shanghai, China, *Aerosol Air Qual.*
897 *Res.*, 10.4209/aaqr.2013.03.0064, 2014.

898 Wang, M., Shao, M., Lu, S.-H., Yang, Y.-D., and Chen, W.-T.: Evidence of coal combustion
899 contribution to ambient VOCs during winter in Beijing, *Chin. Chem. Lett.*, 24, 829-832,
900 10.1016/j.ccllet.2013.05.029, 2013.

901 Wang, M., Shao, M., Chen, W., Lu, S., Liu, Y., Yuan, B., Zhang, Q., Zhang, Q., Chang, C. C.,
902 Wang, B., Zeng, L., Hu, M., Yang, Y., and Li, Y.: Trends of non-methane hydrocarbons (NMHC)
903 emissions in Beijing during 2002–2013, *Atmos. Chem. Phys.*, 15, 1489-1502,
904 10.5194/acp-15-1489-2015, 2015.

905 Wang, Q., Li, S., Dong, M., Li, W., Gao, X., Ye, R., and Zhang, D.: VOCs emission characteristics
906 and priority control analysis based on VOCs emission inventories and ozone formation potentials in
907 Zhoushan, *Atmos. Environ.*, 182, 234-241, 2018.

908 Wang, T., Xue, L., Brimblecombe, P., Lam, Y. F., Li, L., and Zhang, L.: Ozone pollution in China:
909 A review of concentrations, meteorological influences, chemical precursors, and effects, *Sci. Total*
910 *Environ.*, 575, 1582-1596, 10.1016/j.scitotenv.2016.10.081, 2017b.

911 Wang, X.-m., Sheng, G.-y., Fu, J.-m., Chan, C.-y., Lee, S.-C., Chan, L. Y., and Wang, Z.-s.: Urban
912 roadside aromatic hydrocarbons in three cities of the Pearl River Delta, People's Republic of China,
913 *Atmos. Environ.*, 36, 5141–5148, 2002.

914 Wei, W., Cheng, S., Li, G., Wang, G., and Wang, H.: Characteristics of ozone and ozone precursors
915 (VOCs and NO_x) around a petroleum refinery in Beijing, China, *J. Environ. Sci.-China*, 26,
916 332-342, 10.1016/s1001-0742(13)60412-x, 2014.

917 Wu, R., and Xie, S.: Spatial Distribution of Ozone Formation in China Derived from Emissions of
918 Speciated Volatile Organic Compounds, *Environ. Sci. Technol.*, 51, 2574-2583,
919 10.1021/acs.est.6b03634, 2017.

920 Xue, Y., Ho, S. S. H., Huang, Y., Li, B., Wang, L., Dai, W., Cao, J., and Lee, S.: Source
921 apportionment of VOCs and their impacts on surface ozone in an industry city of Baoji,
922 Northwestern China, *Sci. Rep.*, 7, 9979, 10.1038/s41598-017-10631-4, 2017.

923 Yan, Y., Peng, L., Li, R., Li, Y., Li, L., and Bai, H.: Concentration, ozone formation potential and
924 source analysis of volatile organic compounds (VOCs) in a thermal power station centralized area:
925 A study in Shouzhou, China, *Environ. Pollut.*, 223, 295-304, 10.1016/j.envpol.2017.01.026, 2017.

926 Yuan, B., Shao, M., de Gouw, J., Parrish, D. D., Lu, S., Wang, M., Zeng, L., Zhang, Q., Song, Y.,
927 Zhang, J., and Hu, M.: Volatile organic compounds (VOCs) in urban air: How chemistry affects the
928 interpretation of positive matrix factorization (PMF) analysis, *J. Geophys. Res.-Atmos.*, 117,
929 n/a-n/a, 10.1029/2012jd018236, 2012.

930 Zhang, Z., Wang, X., Zhang, Y., Lu, S., Huang, Z., Huang, X., and Wang, Y.: Ambient air benzene
931 at background sites in China's most developed coastal regions: exposure levels, source implications
932 and health risks, *Sci. Total Environ.*, 511, 792-800, 10.1016/j.scitotenv.2015.01.003, 2015.

933 Zhu, Y., Yang, L., Chen, J., Wang, X., Xue, L., Sui, X., Wen, L., Xu, C., Yao, L., Zhang, J., Shao,
934 M., Lu, S., and Wang, W.: Characteristics of ambient volatile organic compounds and the influence
935 f biomass burning at a rural site in Northern China during summer 2013, *Atmos. Environ.*, 124,
936 156-165, 10.1016/j.atmosenv.2015.08.097, 2016.

937

938

939